Icarus 280 (2016) 139–157

Contents lists available at ScienceDirect

Icarus

journal homepage: www.elsevier.com/locate/icarus

Automated localisation of Mars rovers using co-registered HiRISE-CTX-HRSC orthorectified images and wide baseline Navcam orthorectified mosaics

Yu Tao*, Jan-Peter Muller, William Poole

Imaging Group, Mullard Space Science Laboratory, University College London, Holmbury St. Mary, Dorking, Surrey RH5 6NT, UK

ARTICLE INFO

Article history:
Received 22 June 2015
Revised 17 June 2016
Accepted 20 June 2016
Available online 25 June 2016

Keywords:
Mars
Surface
Co-registration
Multi-resolution
Optical localisation
Rover

ABSTRACT

We present a wide range of research results in the area of orbit-to-orbit and orbit-to-ground data fusion, achieved within the EU-FP7 PRoVisG project and EU-FP7 PRoViDE project. We focus on examples from three Mars rover missions, i.e. MER-A/B and MSL, to provide examples of a new fully automated offline method for rover localisation. We start by introducing the mis-registration discovered between the current HRSC and HiRISE datasets. Then we introduce the HRSC to CTX and CTX to HiRISE co-registration workflow. Finally, we demonstrate results of wide baseline stereo reconstruction with fixed mast position rover stereo imagery and its application to ground-to-orbit co-registration with HiRISE orthorectified image. We show examples of the quantitative assessment of recomputed rover traverses, and extensional exploitation of the co-registered datasets in visualisation and within an interactive web-GIS.

1. Introduction

Localisation knowledge of rover position is critical to better path planning and navigation as well as improving the understanding of the geological and morphological context of past, on-going, and planned future Mars rover missions. In the first Mars rover mission in 1997 called Mars Pathfinder (MPF), rover localisation was done via dead reckoning with wheel encoders and a solid-state turn rate sensor. The small rover position and orientation are recognized via lander imagery and updated on a daily base (Matthies et al., 1995). This early local approach could achieve an accuracy of about 10 per cent of the distance from the lander, on top of the uncertainty of the landing site location. Early global approaches include a UHF two-way Doppler tracking system, in which the rover position is determined within an expected accuracy of 50 m (Guinn, 2001), due to the rover-to-orbit geometry changing. Other orbital global methods use triangulation of telemetry data and identified landmarks that appeared in both ground and orbital imagery which can achieve an accuracy of close to 100 m (Li et al., 2004).

In the Mars Exploration Rover (MER) mission, rover position and orientation were calculated via wheel odometry, Sun finding, and an onboard Inertial Measurement Unit (IMU). Visual odometry algorithms (Xu et al., 2001) and Incremental Bundle Adjustment (IBA) algorithms (Li et al., 2004) were developed at the Jet Propulsion Laboratory (JPL) and Ohio State University (OSU), focusing on onboard positioning and offline processing, respectively. Another approach is through manual correlation of ortho-projected rover imagery and HiRISE ortho-image in the selected best tactical places which has been employed in the Mars Science Laboratory (MSL) mission (Parker et al., 2013).

The optimised localisation method, which has been widely used in the MER mission, is IBA. IBA takes a global approach by building an image network of the landing site (Li et al., 2005). IBA uses the initial location and heading information from the telemetry data or improved visual odometry results to compute refined Exterior Orientation (EO) parameters of all images progressively from the starting sol 1 upon landing along with the landing site position. The success of IBA depends heavily on the Tie-points (TPs) that are used to connect the rover images, usually from for and aft-looking Navcam images (Li et al., 2004). A rover can be localised to an accuracy of about 2% of the distance from the lander and ideally an accuracy of 0.1% of the total traverse length if the traverse leg length (distance between stations) is less than 60 m.

However, this image network based methods do not guarantee compliance of rover and global aerographic co-ordinates, because

* Corresponding author.
E-mail addresses: yu.tao@ucl.ac.uk (Y. Tao), j.muller@ucl.ac.uk (J.-P. Muller), william.poole.10@ucl.ac.uk (W. Poole).

http://dx.doi.org/10.1016/j.icarus.2016.06.017

Table 1
Sources of HRSC, CTX and HiRISE ORI/DTM production.

Dataset	Source ID	ORI and DTM producer	ORI and DTM resolution
MER-A HiRISE	PSP-001513-1655 PSP-001777-1650	OSU	0.25m 1m
MER-A CTX	B18-016677-1653-XN-14S184W G01-018523-1653-XI-14S184W	UCL	6m 18m
MER-A HRSC	h4165-0000-nd4	DLR v50	12.5m 75m
MER-B HiRISE	PSP-009141-1780 PSP-001414-1780 ESP-011765-1780 ESP-012820-1780 ESP-021536-1780 PSP-004289-1780 PSP-010341-1775 PSP-010486-1775	OSU	0.33m 1m
MER-B CTX	B22-018134-1779-XN-02S005W G01-018490-1779-XN-02S005W	UCL	6m 18m
MER-B HRSC	h1183-0000-nd4	DLR v53	12.5m 100m
MSL HiRISE	PSP-010639-1755 PSP-010573-1755	USGS	0.25m 1m
MSL CTX	P21-009149-1752-XI-04S222W P21-009294-1752-XI-04S222W	UCL	6m 18m
MSL HRSC	h1927-0000-nd4	DLR v52	12.5m 50m

EO adjustment of positions along the traverse was performed incrementally based on the initial landing site location. In this study, we demonstrate an automated global method to localise the rover positions via co-registration of bundle adjusted wide baseline rover ortho-rectified image (ORI) and corresponding High Resolution Image Science Experiment (HiRISE) ORI, which itself is co-registered to Mars Reconnaissance Orbiter (MRO) Context Camera (CTX) data, hence to High Resolution Stereo Colour Imager (HRSC) data, and finally tied to 3D position via a reference network of Mars Orbiter Laser Altimeter (MOLA) locations.

The work commenced with the automated co-registration of common features in the orbital datasets, consisting of ORIs and Digital Terrain Models (DTMs) with respect to the surface missions, MER-A, MER-B and MSL. Automated HiRISE-CTX-HRSC co-registration is performed via global least square fitting based on mutual shape adapted automated tie-points (Tao and Muller, 2013). The co-registration accuracy achieved is up to the sub pixel level of the finer layer, e.g. 60 cm/pixel for CTX-to-HRSC and 25 mm/pixel for HiRISE-to-CTX. The co-registered multi-level maps are then used as an image map base for ground-to-orbit fusion. In the second stage, we produce 1 cm/pixel wide baseline ORI/DTM from Navcam stereo images via region growing/ALSC (Shin and Muller, 2012) based on overlap between left and right images of a pair (intra-stereo) and Bundle Adjustment (BA) for overlap between neighbouring image pairs (inter-stereo). In the final stage, we fuse the reconstructed wide baseline ground ORI/DTMs with HiRISE ORI/DTMs to bring the high-resolution ground products into a common global context and therefore to update the rover positions. The ground-to-orbit co-registration is performed via a combined mutual information/morphological edge extraction method and cross-validated using rover tracks that appear on different HiRISE images, which are similarly co-registered with each other and CTX/HRSC. In cases where a sufficient number of HiRISE images are available, super-resolution restoration is used to build a higher resolution ORI for subsequent fusion with the rover ORI mosaics.

This paper describes the localisation results achieved within the EU-FP7 Planetary Robotic Vision Ground Processing (PRoVisG) project[1] which ran from October 2008 to June 2012 and the EU-FP7 Planetary Robotic Vision Data Exploitation (PRoViDE) project[2] that started in 2013 to collect all the multi-view imaging data from ground level robotic and orbital sensors covering three Mars rover missions (MER-A, MER-B, MSL), and process them into a coherent set of co-registered 3D imaging products (Paar et al., 2013). We further introduce our interactive 3D viewer and the web-GIS system (PRoGIS) developed initially at UCL and later extended with colleagues at the University of Nottingham particularly for visualisation and scientific analysis of the data and processed products from orbital context to rover imagery in co-registered global geo-context. We demonstrate that these tools will not only initiate better scientific understanding of the surface of Mars for experts, but also serve the educational, public outreach and scientific objectives of our research (Morley et al., 2014).

2. Orbital data processing

2.1. MOLA, HRSC, CTX, HiRISE ORI/DTM overview

The global reference of our localisation work is MOLA data, which is considered as the best global Mars 3D reference model in the 1990s acquired to date. Individual MOLA tracks have been interpolated and extrapolated to yield a global MOLA DTM with a spatial resolution of up to 128 grid-points per degree (≈460 m) and vertical resolution of 2–13 m.

DLR have generated along-track orbital strip DTMs (at grid-spacing from 50–150m) and ORIs (up to 12.5 m/pixel) by processing the raw HRSC data using radiometric de-calibration, noise removal, image matching, geo-referencing, photogrammetric data processing, and where these have been employed along-track BA, they are then labelled as Level-4 Version 50+ when the products reach a satisfactory level of quality (Scholten et al., 2005). The v50+ HRSC DTMs use the MOLA reference sphere with a radius of 3396.0 km. In this work, v50+ HRSC ORI/DTM has been employed as a reference base map for subsequent cascaded CTX/HiRISE co-registration.

The MRO Context Camera is currently capturing greyscale images at ≈ 6 m/pixel over a swath-width of 30 km. We have processed CTX stereo pairs as shown in Table 1 to derive ORI and DTM of 18m/grid point resolution, using the NASA Ames Stereo Pipeline (ASP), which is publicly available (Broxton and Edwards, 2008) as an extension of the USGS ISIS system. CTX is used to reduce the resolution gap from HRSC to HiRISE data. For MER-A, B, we employ the HiRISE ORI/DTM and ORI/DTM mosaics produced by our US collaborators from the mapping and GIS Laboratory, Ohio State University (OSU). They reported their rigorous photogrammetric model for HiRISE and coarse-to-fine hierarchical matching approach in Li et al. (2011). They are processed from stereo pairs as listed in Table 1 and the products have a spatial

[1] http://provisg.eu.
[2] http://provide-space.eu.

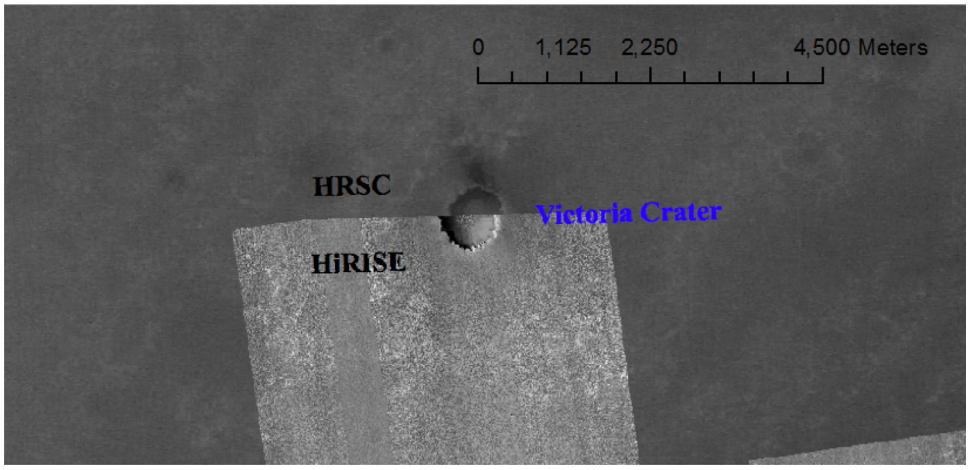

Fig. 1. Example swipe view showing mis-registration between HiRISE ORI mosaic and HRSC (co-registered with MOLA) at Victoria Crater, MER-B. North is up.

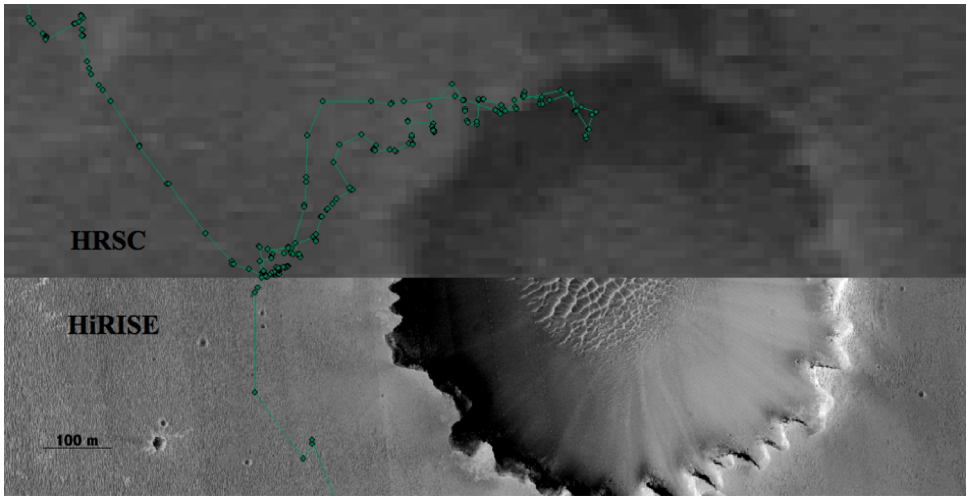

Fig. 2. Example of co-registered HiRISE and HRSC ORIs at Victoria Crater: showing clearly that the MER-B traverse (green line) does not fit the HRSC ORI and no longer fits the HiRISE after co-registration to HRSC ORI. North is up.

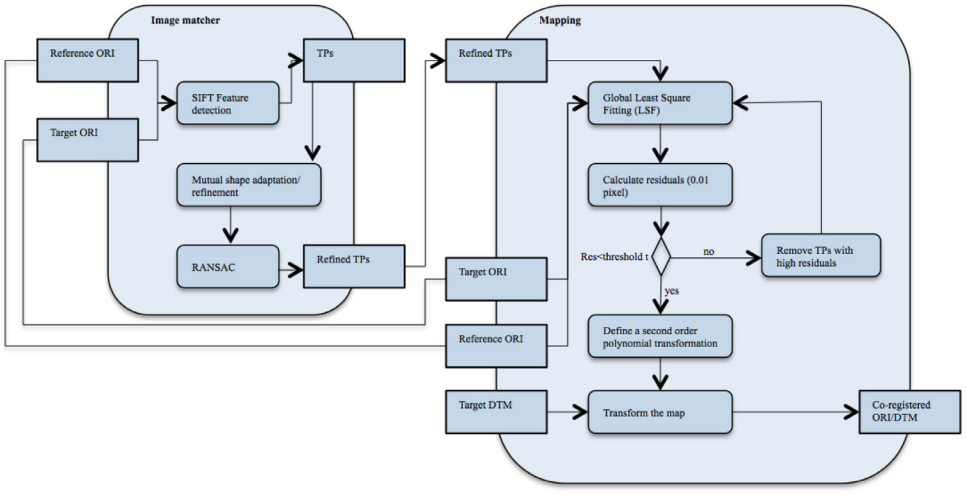

Fig. 3. Flow diagram of the HiRISE-CTX-HRSC co-registration processing chain.

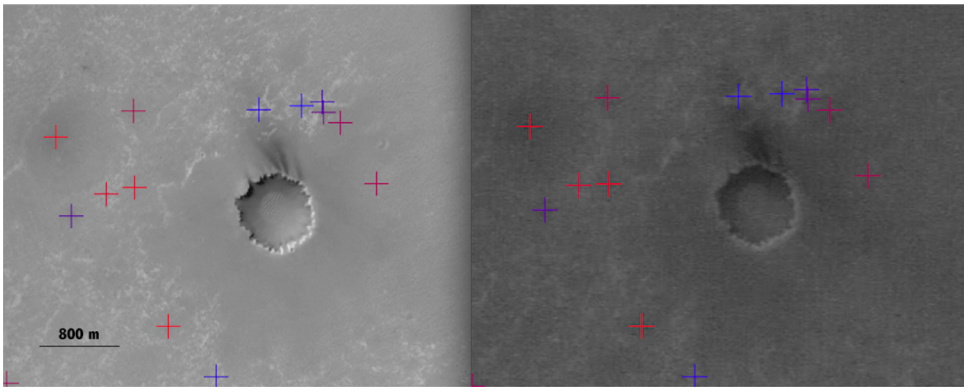

Fig. 4. Example of detected TPs (showing from red to blue with increasing similarity values for MER-B CTX ORI (left) and HRSC ORI (right) at Victoria Crater. (For interpretation of the references to colour in this figure legend, the reader is referred to the web version of this article).

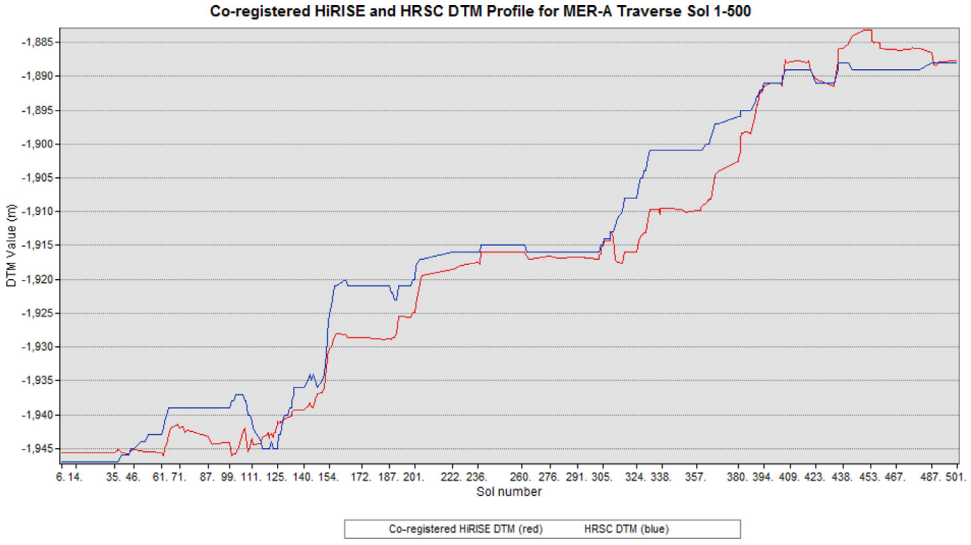

Fig. 5. DTM profile for co-registered MER-A HiRISE (red) and HRSC (blue) along rover traverse from sol 1 to 500. (For interpretation of the references to colour in this figure legend, the reader is referred to the web version of this article).

Table 2
RMSE (in pixel) from Auto TPs and Manual CPs.

Datasets (Num of TPs/CPs)	Auto TPs RMSE Avg. (pixel)	Auto TPs RMSE Max. (pixel)	Manual CPs RMSE Avg. (pixel)	Manual CPs RMSE Max. (pixel)
MER-A HRSC-CTX (411/36)	0.0145	0.0486	1.7697	2.6611
MER-A CTX-HiRISE (325/36)	0.0073	0.0252	0.8695	1.2124
MER-B HRSC-CTX (994/81)	0.0471	0.1734	2.7707	3.6165
MER-B CTX-HiRISE (179/81)	0.0430	0.1390	0.3162	1.0382
MSL HRSC-CTX (52/36)	0.0124	0.0319	0.9114	2.1344
MSL CTX-HiRISE (2562/36)	0.0056	0.0093	0.6548	1.3201

resolution of 25 cm for a single strip MER-A HiRISE ORI, 33 cm for MER-B HiRISE ORI Mosaic, and 1 m/grid point for the DTMs. For MSL, we use the HiRISE ORI/DTM produced by the U.S. Geological (USGS) Astrogeology team using ISIS and SOCET SET software

Table 3
MER and MSL stereo camera specifications.

Stereo Cameras	MER Pancam	MER Navcam	MSL Navcam	MSL 34mm Mastcam	MSL 100mm Mastcam
Stereo Base (cm)	30	20	42.4	n/a	n/a
Focal Length (mm)	38	14.67	14.67	34	100
Field of View (deg)	16	45	45	15	5.1
Angular Resolution (mrad/pixel)	0.28	0.82	0.82	0.22	0.074

(Kirk et al., 2008). The spatial resolution is 25 cm for MSL HiRISE ORI and 1 m/grid point for the DTM.

The availability of HiRISE images has brought the global surface localisation work to a new level of accuracy. However, when taking a closer look to the HiRISE ORI/DTM (from the NASA[3] and UA[4] HiRISE site) and HRSC ORI/DTM (DLR processed v50+ products), we found that they are not well co-registered to each other, as shown in Fig. 1. There are mis-registrations of about 100 m be-

[3] http://pds-imaging.jpl.nasa.gov/.
[4] https://hirise.lpl.arizona.edu/.

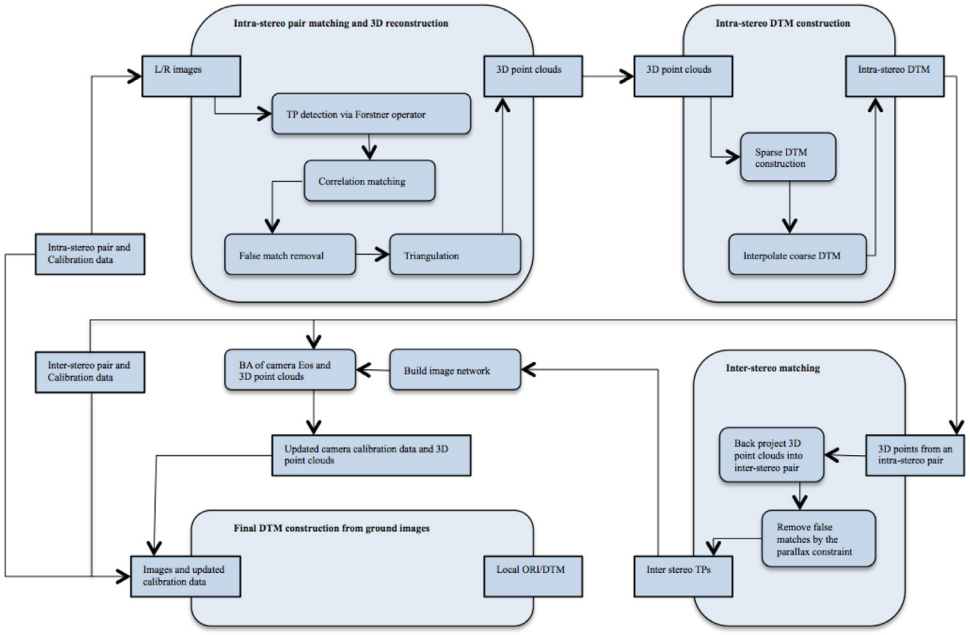

Fig. 6. Flow diagram approximating OSU's MER landing site mapping processing chain based on Li et al. (2006).

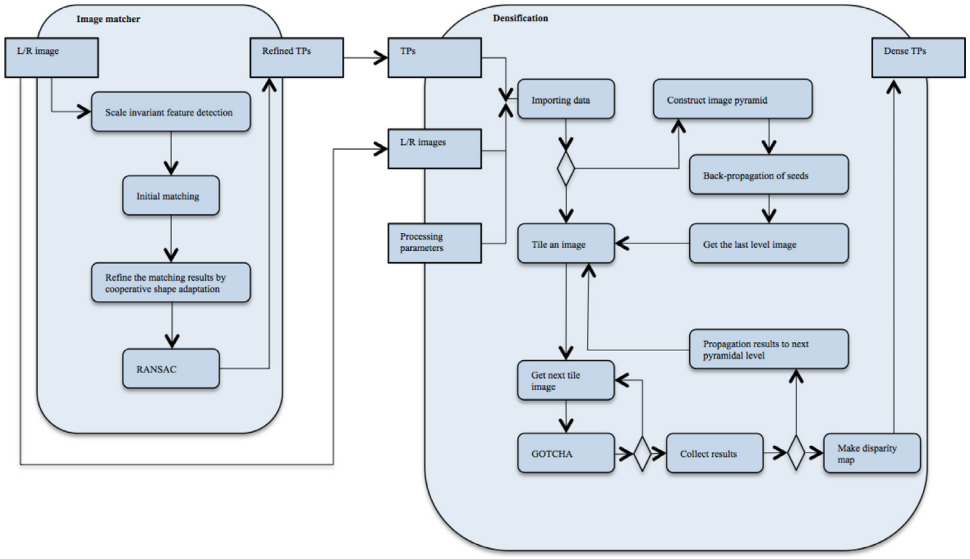

Fig. 7. Flow diagram of our matcher used for wide baseline stereo reconstruction.

tween HiRISE and HRSC for MER-A, 100–150 m for MER-B between HiRISE and HRSC, and 100–200 m for MSL HiRISE and HRSC, according to manually selected control points on obvious landmark features, such as crater edges. After selecting homologous tiepoints and applying a second order transformation, the mis-registration can be reduced to pixel level (Poole and Muller, 2013). However, this had the unintended consequence that the rover traverses, which were corrected with respect to the landing site location using look-ahead/behind optical navigation, IBA (Li et al., 2006), no longer fitted on the HiRISE map, as shown in Fig. 2. It became obvious when trying to place rover traverses (MER and MSL) in context that such traverses did not match with known landmarks visible in the orbital images. The mis-registration is negligible from a global perspective but could cause a huge offset when trying to locate rover positions in a global context. Even manually registered HiRISE/HRSC dataset showed up to 10–50m offset of the initial landing site location. The offset accumulates while the rover moves further away from the original landing site location. Therefore, we take CTX ORI as a resolution bridge, applying an automated tiepointing method to co-register the HiRISE and HRSC datasets. The co-registration accuracy has been improved from pixel level to subpixel level (Poole and Muller, 2013, Tao and Muller, 2013).

2.2. Local and global reference systems

There are two primary reference systems used in localisation, the landing site local reference system and the Mars global reference system. In the landing site local reference system, the origin is fixed with respect to the spacecraft. The Surface Fixed Coordinate System (SFC) is one of the landing site local reference

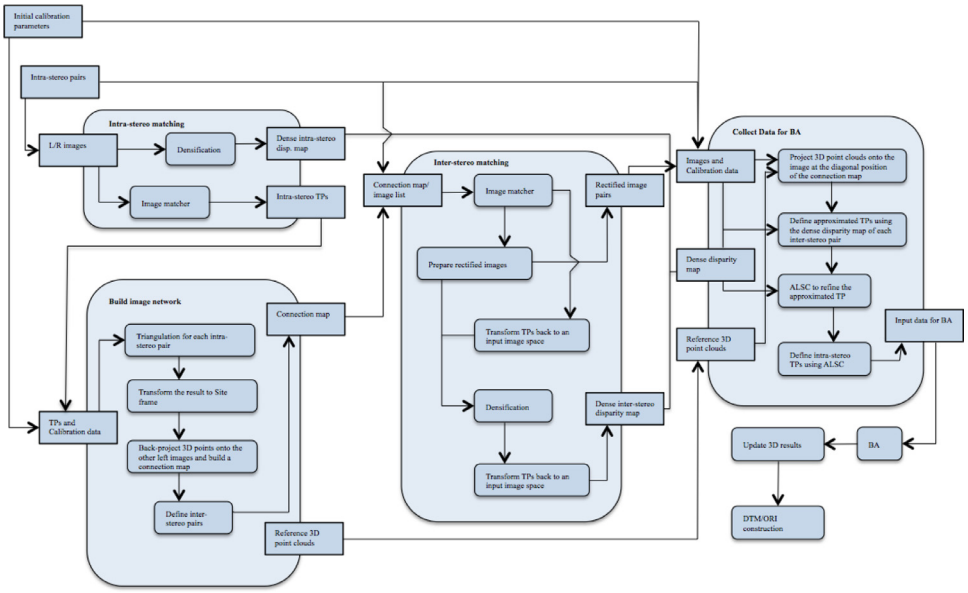

Fig. 8. Flow diagram of our wide baseline stereo reconstruction processing chain.

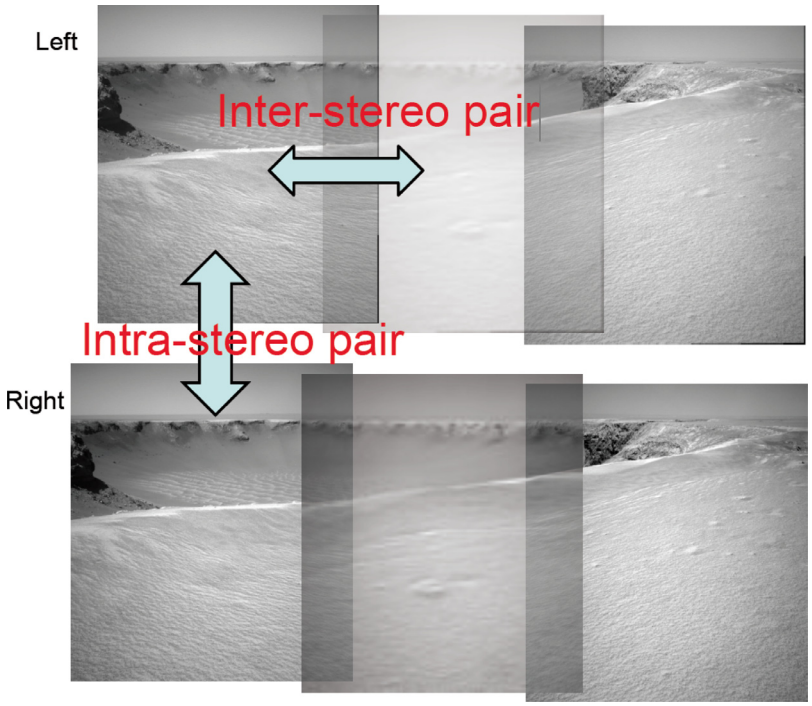

Fig. 9. Example of Navcam stereo images of MER-B near to Victoria crater on sol 951 illustrating intra-stereo and inter-stereo: top shows Navcam left eye mosaic, bottom shows Navcam right eye mosaic. Inter-stereo refers to stereo produced from the overlap in two images from the same camera, while intra-stereo refers to stereo generated from the parallax between the two camera eyes.

systems, in which the X-axis lies on the tangent plane at the origin and points to the North Pole, the Z-axis points down in the normal direction of the martian ellipsoid, and the Y-axis is formed in the right-handed system (Li et al., 2004). Another landing site local reference system is the Landing Site Cartographic Coordinate System (LSC). LSC is an east-north-up (X-Y-Z) right-handed local system and can be converted to SFC with a set of axis rotations.

Landing site local reference systems are widely used in image network based localisation methods. The origin of the MER-A local reference system, i.e. the lander location for MER-A Spirit (Columbia Memorial Station), was determined as 14.571892°S, 175.47848°E (Guinn and Ely, 2004) via fitting direct-to-Earth (DTE) two-way X-band Doppler signals and two passes of UHF two-way Doppler signals between Spirit and the Mars Odyssey orbiter. The origin was further corrected to 14.5692°S, 175.4729°E (Parker et al., 2004) via optimal triangulation of lander panoramas and the JPLs Descent Image Motion Estimation System (DIMES) and Mars Orbiter Camera (MOC) Narrow Angle (NA) images. The origin of the MER-B local reference system (Eagle Crater) was determined

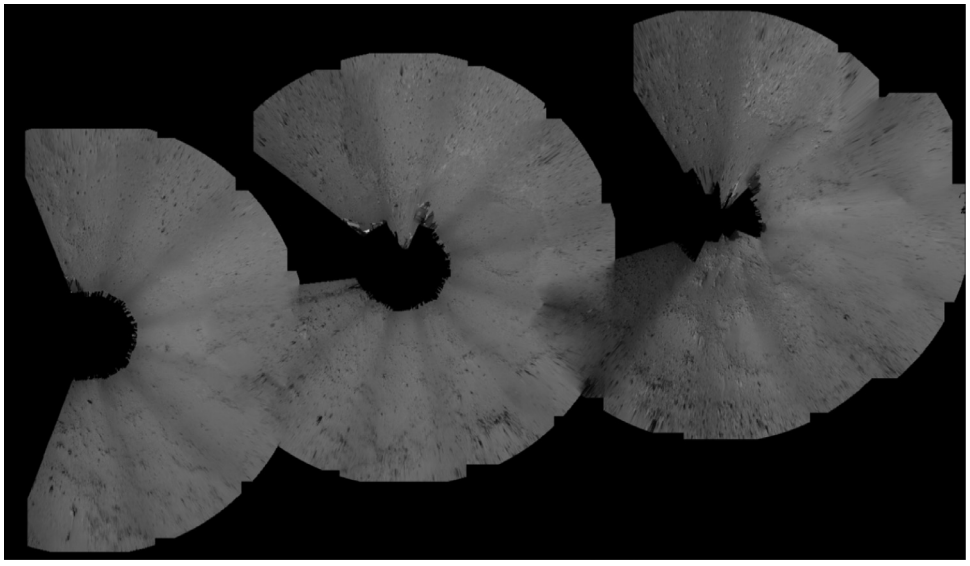

Fig. 10. An example of MSL Navcam ORI mosaic for Sol 50–54 that cannot be used for automated Navcam to HiRISE co-registration because of lacking structural features. North is up.

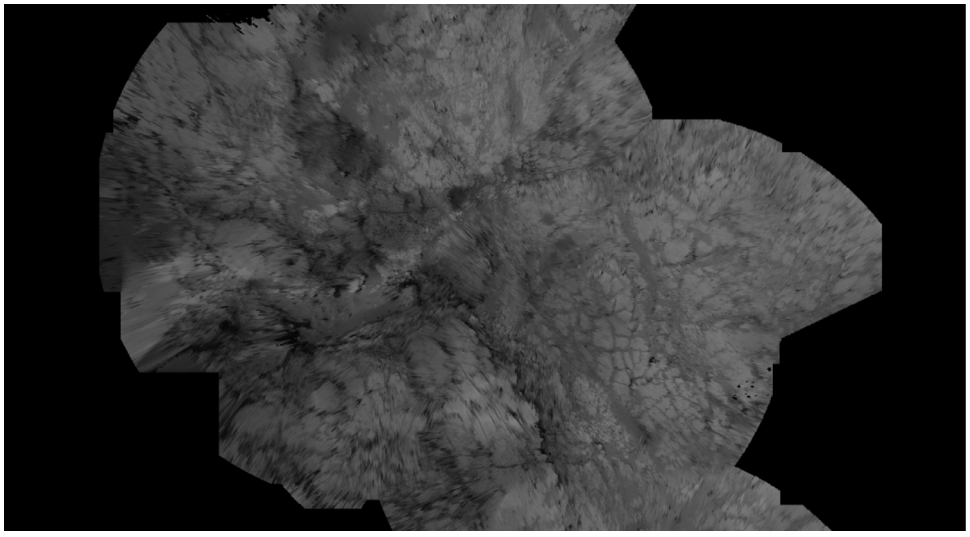

Fig. 11. An example of MSL Navcam ORI mosaic for Sol 127–131 that contains rich structural features and can be used for automated Navcam to HiRISE co-registration. North is up.

as 1.948282°S, 354.47417°E (Guinn and Ely, 2004) via the UHF two-way Doppler system and corrected as 1.9462°S, 354.4734°E (Parker et al., 2004) via triangulation to three craters observed in both the lander panorama and the DIMES descent and MOC NA images. By 2010, as more CTX and HiRISE images became available, the lander locations were further updated to 14.5709°S, 175.4797°E for MER-A and 1.9470°S, 354.4717°E for MER-B via a manual procedure to compare image features identified on both the Mars Orbiter Camera (MOC) and HiRISE images (Li et al., 2010). However, we found that the landing site coordinates are still not precise with respect to MOLA data according to the HiRISE images, which are co-registered with HRSC and MOLA. The rover reference origins are localised to 14.571166°S 175.478431°E for MER-A, and to 1.94726865°S 5.52413974°W for MER-B in our approach which will be illustrated in the following sections.

On the other hand, the global reference system includes the Inertial Reference System and the Mars Body-Fixed (MBF) Reference System. The MBF system defines either a spherical coordinate system using planetocentric latitude and longitude toward the east, or an ellipsoidal coordinate system using planetocentric latitude and longitude toward the west. The MOLA datasets adopted the use of planetocentric latitude and east longitude global reference system. Due to the higher accuracy and detailed information of the MOLA products, the MRO mission adopted the same system, i.e. Mars 2000, defined by the International Astronomical Union/International Association of Geodesy (IAU/IAG).

2.3. Automated tie-point based co-registration

In this work, we start with projecting the CTX and HiRISE ORI/DTM from the Mars 2000 geographic coordinate system into the Sinusoidal projection system with the same central meridian value, which is originally used in the HRSC v50+ datasets. For MER-A, the central meridian is 176°E, MER-B is 354°E and MSL is 138°E. The sinusoidal projection system is a systematic transformation of the latitudes and longitudes of locations on the surface of a sphere

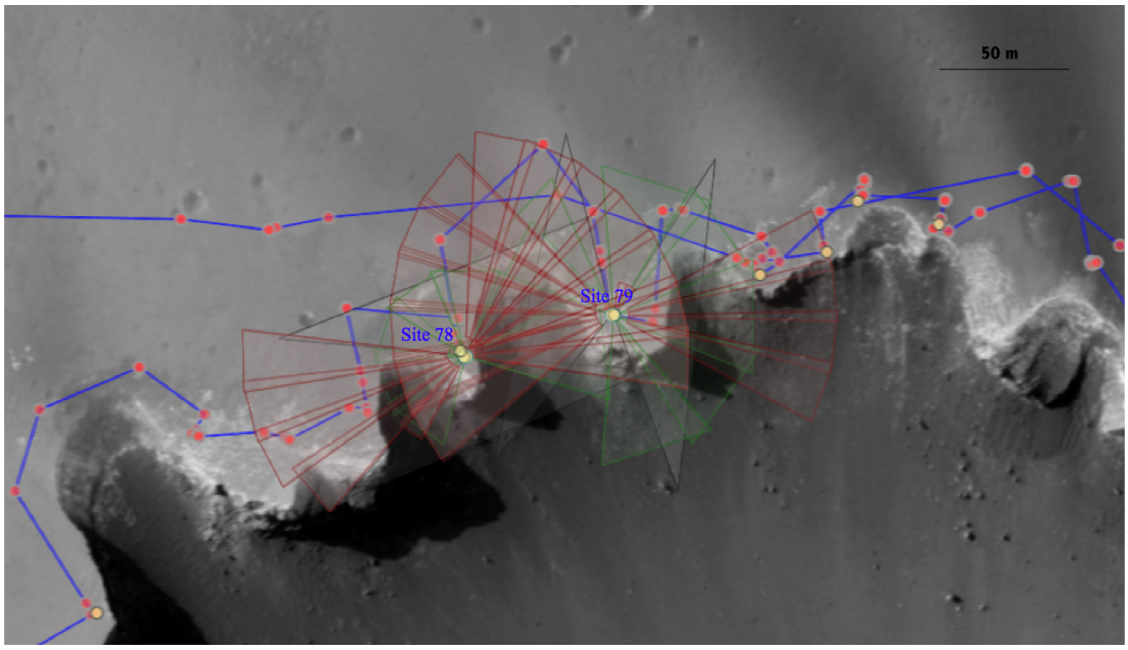

Fig. 12. Visual fulcra of Site 78 and 79 at Victoria Crater showing intersections between Pancam (red) and Navcam (green) view on these two sites taken from PRoGIS (Morley et al., 2014). The blue lines are rover traverse and the red dots are rover stops. North is up. (For interpretation of the references to colour in this figure legend, the reader is referred to the web version of this article).

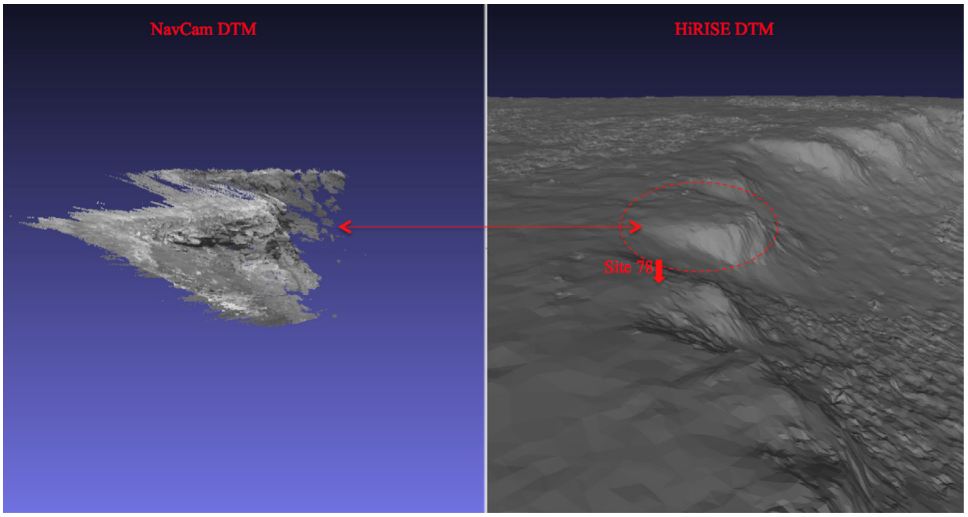

Fig. 13. Reconstructed MER-B wide baseline Navcam DTM and HiRISE DTM at Victoria Crater in 3D showing possibilities of registration of different resolution 3D point clouds in one particular area that the rover goes into the crater.

or an ellipsoid into locations on a plane. We then apply a global least square fitting transform based on mutual shape adapted automated tiepoints. The processing chain is shown in Fig. 3.

The processing starts with detection of Scale Invariant Feature Transform (SIFT) feature points. SIFT is widely used in image matching/registration in computer vision. However, the general feature-based matching methods assume that the image features that are detected independently on each image are always correct. The repeatability of the detection would be deteriorated when a significant distortion is involved in a matching (target) image. Slight mismatches could result in a significant impact on the global transformation. Therefore, we developed a Mutual Shape Refinement (MSR) algorithm that combines the scale and affine invariant feature detector with Adaptive Least Square Correlation (ALSC) to refine the matching result iteratively and obtain more accurate TPs.

The algorithm of mutual shape refinement consists of 6 steps: (i) Detect a scale invariant feature and its scale; (ii) Iteratively update a circular scale invariant region to an elliptical region using the second moment matrix; (iii) Initial normalisation using the result from ii. (iv) Refine the result using forward and backward ALSC on both images; (v) Go back to iv until it converges (optional); (vi) Go back to ii until it converges (optional, not necessary). Fig. 4 shows an example of detected TPs for MER-B CTX and HRSC ORIs at Victoria crater.

The next step is to define a 2nd order polynomial transformation from the refined TPs. The transformation is decided according to the Least Square Fitting (LSF) algorithm and adjustment of local

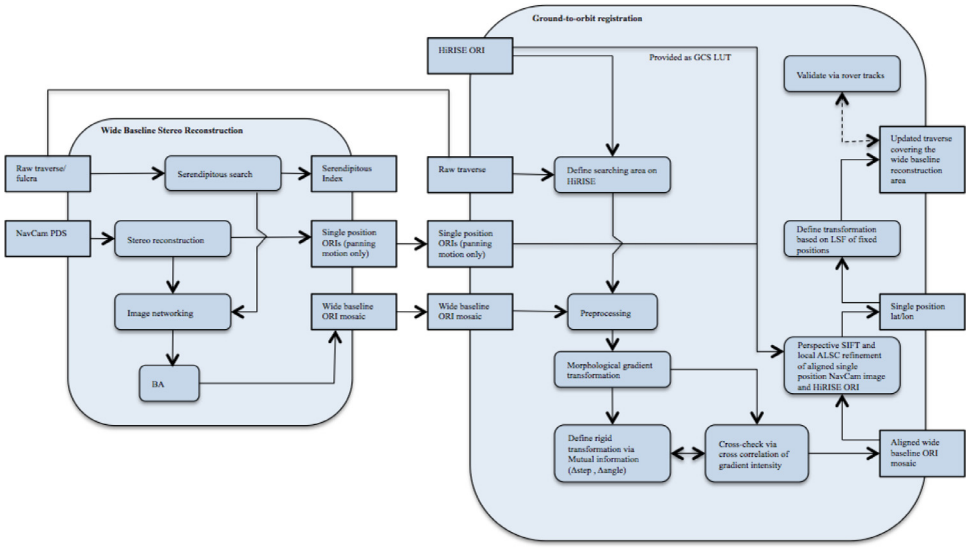

Fig. 14. Flow diagram of our ground-to-orbit fusion processing chain.

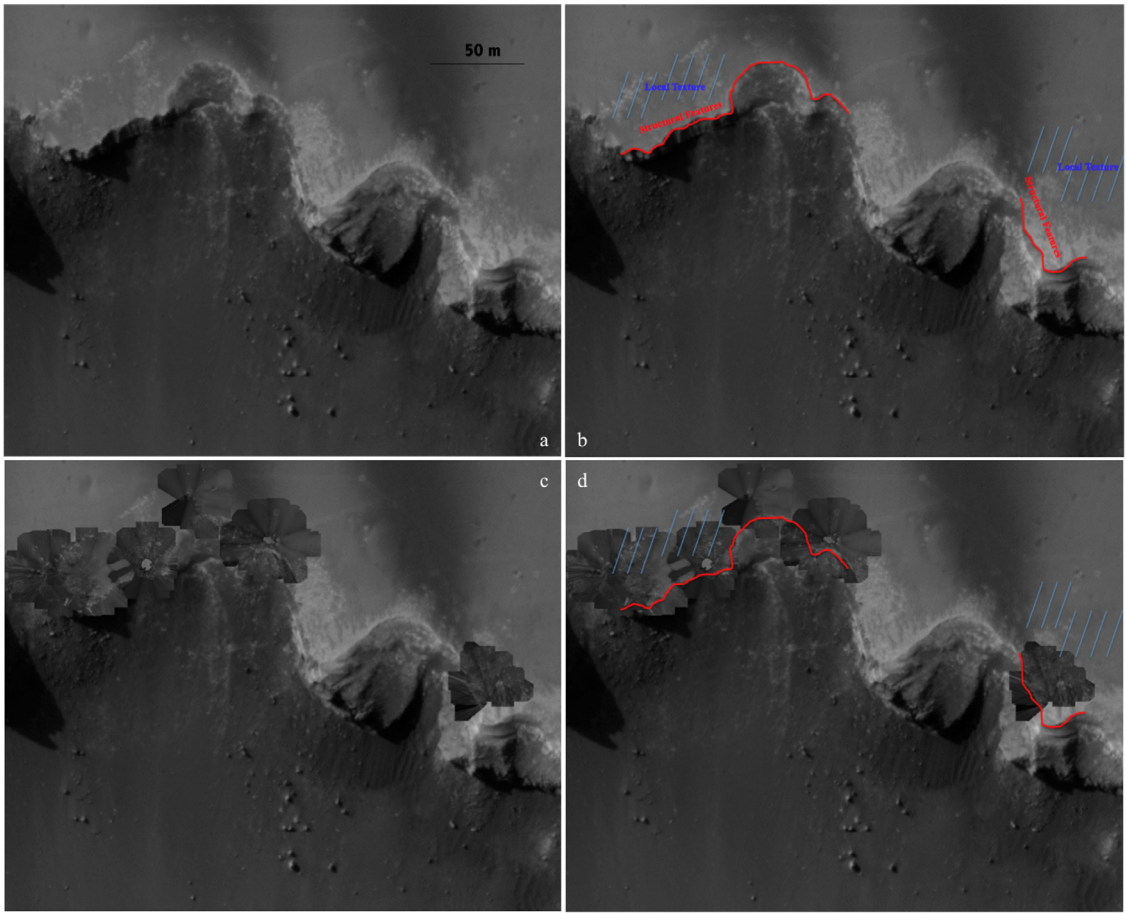

Fig. 15. Example of "structural feature" (red line) and "local texture" (blue cross) on HiRISE ORI (a, b) and wide baseline Navcam ORI co-registered and superimposed with HiRISE ORI (c, d) at Site 80 to 82 at Victoria Crater. North is up. (For interpretation of the references to colour in this figure legend, the reader is referred to the web version of this article).

TPs to a better fitting of the global TPs using Triangulated Irregular Network (TIN) interpolation. The residuals are calculated iteratively and outliers removed until a threshold is reached. The final transformation for the ORIs is then applied to the DTMs. Consistency is checked from both reference-to-target and target-to-reference back-matching and in comparison with the approaches reported in Kim and Muller (2009) for DTM co-registration at UCL-MSSL.

The co-registration was performed for HiRISE, CTX, and HRSC (registered with MOLA) for MER-A, MER-B, and MSL rover missions. The co-registered datasets act as the reference set for the

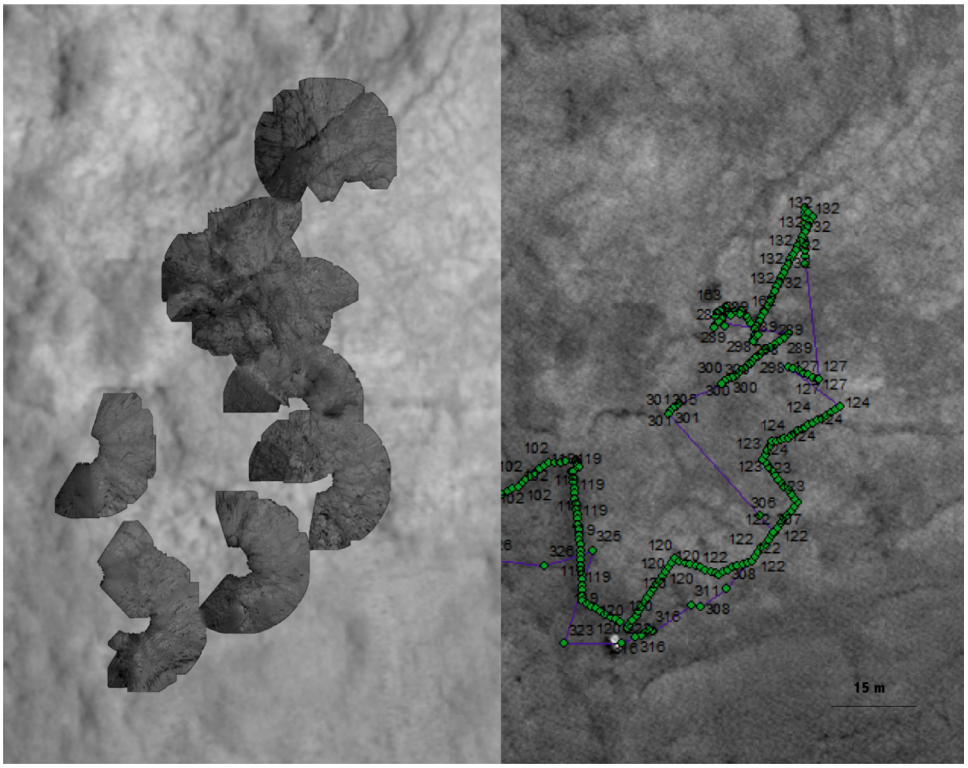

Fig. 16. Example of co-registered wide baseline Navcam ORI and HiRISE ORI (left) and corrected traverse (right) for MSL from Sol 120 to 179 shown in green dots and purple lines. North is up. (For interpretation of the references to colour in this figure legend, the reader is referred to the web version of this article).

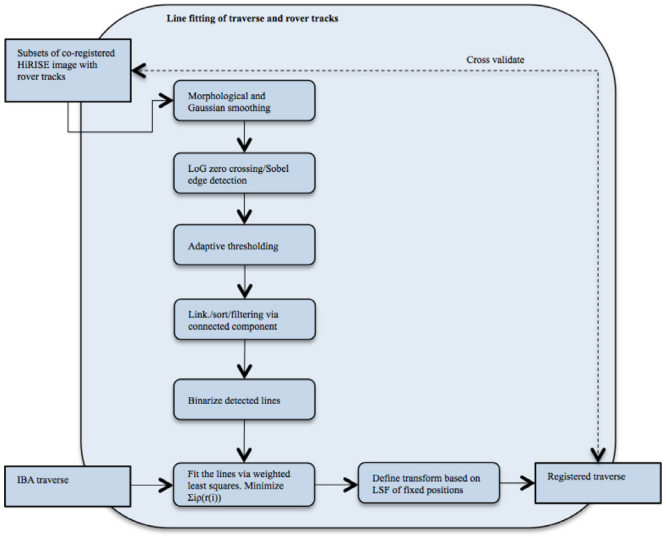

Fig. 17. Flow diagram of the alternative line fitting methods for "difficult areas" in MER-A localisation.

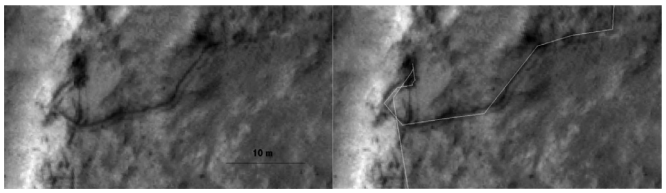

Fig. 18. Rover tracks on MER-A HiRISE image (PSP-010097-1655) and fitted rover traverse (white lines) at HomePlate. North is up.

co-registration of reconstructed wide baseline ground ORIs, which is described in a later section.

2.4. Assessment of HRSC-CTX-HiRISE co-registration

During the transformation decision stage, we iteratively minimize the residuals for all selected TPs. In the first iteration, TPs with large residuals (> 10 pixels) were removed. Then residuals are minimised to less than 0.5 pixels after 3–5 iterations. A large number of highly correlated TPs ensure a sub-pixel level of matching accuracy. A quantitative evaluation of the automatically detected feature points (TPs) and manually selected control points (CPs) has been taken for all three sets of dataset. The Root Mean Sqaure Error (RMSE) in pixels for auto TPs and manual CPs are calculated as an intrinsic measurement of the auto co-registration process. Table 2 shows the statistics of the residuals of automated TPs compared with manually selected CPs for HRSC to CTX and CTX to HiRISE co-registration. The first column indicates the datasets and total number of TPs/CPs used in this evaluation. Since we are using a global LSF adjustment method, which introduced local transformation, the residuals of auto TPs are comparably low from 0.0056 pixels for MSL CTX-HiRISE co-registration to 0.0471 pixels for MER-B HRSC-CTX co-registration. Manual CPs are selected on viewable features, e.g. corners, line intersections, high local curvature points. They are relatively evenly distributed using a grid pattern to define the spatial distribution based either a 5-by-5 grid (36 CPs in total) for MER-A and MSL or a 8-by-8 grids (81 CPs in total) for MER-B. It is impossible to find an absolutely even distribution of CPs in flat featureless areas, however, in this way, evaluation on selected CPs will take into consideration any local distortions caused by LSF transformation.

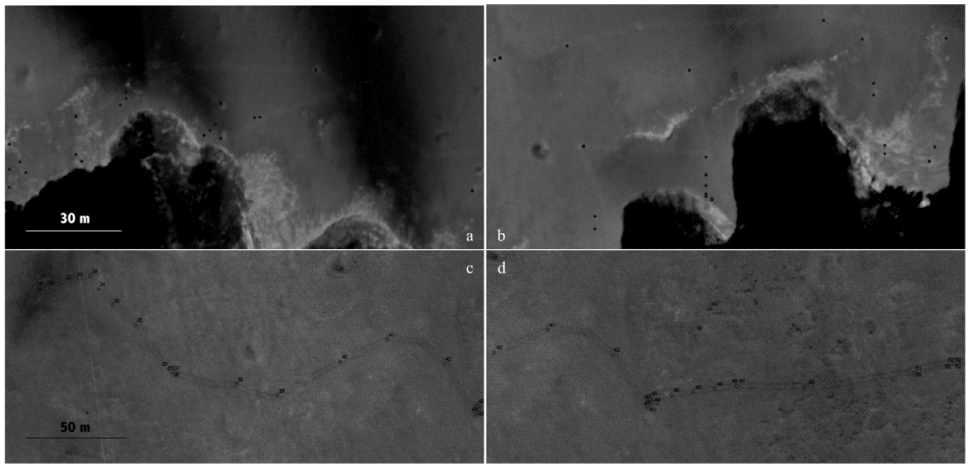

Fig. 19. Co-registered rover positions on MER-B (a, b) and MSL (c, d) HiRISE ORI showing alignment of the corrected traverse and rover tracks. North is up.

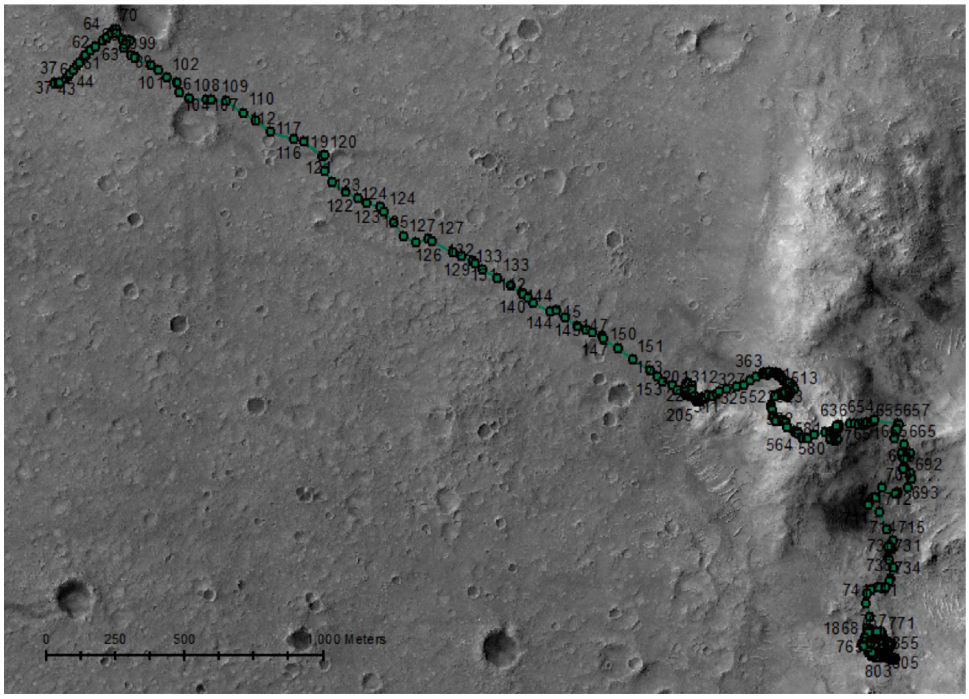

Fig. 20. Corrected MER-A rover traverse (green) on HiRISE ORI (co-registered with CTX, HRSC, MOLA). North is up. (For interpretation of the references to colour in this figure legend, the reader is referred to the web version of this article).

The average RMS error of HRSC-CTX on manual CPs is higher mainly due to the larger resolution difference between these two datasets.

At the final level, the ORI-based co-registration results were evaluated using the corresponding DTM elevations in 10 test regions with different terrain types. These 10 test regions were selected along or around the rover trajectory for each mission. The elevation profiles from HRSC and HiRISE DTMs show a high level of consistency with the linear interpolation of the corresponding HRSC DTM elevations. Fig. 5 shows an example of the DTM profile for co-registered MER-A HiRISE and HRSC along the rover traverse up until sol 500. The maximum difference found is less than 10 m. Although the ORIs have been co-registered at sub-pixel levels of accuracy with respect to 25 cm resolution of HiRISE ORIs, the elevation difference in the profiles are mainly introduced from the vertical resolution gap and interpolation of 75 m/pixel spatial resolution of the HRSC DTM.

3. Ground data processing

3.1. Stereo cameras onboard MER-A, MER-B, and MSL

The onboard MER Panoramic camera (Pancam) and Navigation camera (Navcam) allow much improved resolution and exploration of the martian surface compared to orbital camera systems. Table 3 has summarised the camera spicifications (Maki et al., 2012; Malin et al., 2010).

Although MER Pancam and MSL Mastcam have a higher inherent resolution for mapping medium to far range objects (up to 20m in range) they have a narrower FOV angle. Therefore,

Fig. 21. Corrected MER-B rover traverse (green) and initial IBA traverse (red) on HiRISE map (co-registered with CTX, HRSC, MOLA). North is up. (For interpretation of the references to colour in this figure legend, the reader is referred to the web version of this article).

Navcam stereo images are considered more suitable for reconstructing wide baseline features that can be correlated with features viewable in orbital imagery. In case of any detailed texture information, the reconstructions from MER Pancam or other 2D science imagers, e.g. Mastcam, MAHLI, ChemCam, can be co-registered with Navcam 3D reconstructions and thereby fit into a global context (Tao and Muller, 2013).

3.2. Wide baseline stereo reconstruction

Due to large scale and viewpoint differences, it is not easy to link a single ground image to corresponding landmarks in an orbital image. Even if possible, the result would not be useful when the coverage of the ground view is too small compared with the orbital global view. Therefore, an alternative is required which uses serendipitous wide baseline imagery and its subsequent 3D reconstruction to link features in ground products with corresponding features in orbital datasets. OSU reported their wide-scale landing site mapping methods in Li et al. (2006). The OSU reconstruction pipeline shown in Fig. 6 includes a Forstner operator and correlation matching based intra-stereo (Xu, 2004) matching step. UCL has a different matcher, shown in Fig. 7 which is based on a tiled region growing-based ALSC (Otto and Chau, 1989). An intra-stereo DTM construction and interpolation process is required because a general correlation matcher cannot deal with affine distortion. The third step is back projecting 3D point clouds onto inter-stereo pairs to build an image network. This assumes that a back-projection transformation from the initial calibration parameters is good enough to get matches. However, this is only true in the case of a panning motion of the same sensor at a fixed rover position. The final step is BA of the camera extrinsic parameters and 3D point clouds. The final DTM can be interpolated using a Kriging method.

A wide baseline reconstruction can be addressed in 3 cases: (1) Panning motion of the same sensor at a fixed rover position. (2) Panning motion of different sensors, i.e. Navcam and Pancam for MER, Mastcam and Navcam for MSL, at a fixed position or a general motion of the same/different sensors, at different rover positions. (3) Cross-site stereo pairs. We only focus on cases 1 and 3, because we considered that multi-sensor fused reconstruction is less efficient in localisation work due to the narrower FOV for MER Pancam and MSL Mastcam compared with Navcam. Large-scale structural information is more useful for fusion with HiRISE ORI compared with the very detailed local texture from MER Pancam and MSL Mastcam.

In the NASA PDS, MER and MSL camera calibration data is defined in the rover coordinate system, while the reconstruction result, i.e. XYZ data, uses the Site coordinate system. A transformation between a rover frame and its site frame can be defined using 7 parameters in the PDS header, i.e. 3 offset and 4 quaternion parameters.

Fig. 8 shows the flow diagram of the wide baseline stereo reconstruction work flow used in this work. The wide baseline stereo reconstruction processing contains 4 stages: (1) Intra-stereo matching; (2) Build image network; (3) Inter-stereo matching; (4) Bundle adjustment of inter-stereo point clouds. Fig. 9 illustrates the terms of intra- and inter-stereo.

We initially use the CAHVOR camera coefficients recorded in the PDS header for intra-stereo reconstruction and building the inter-stereo network. In the first stage, intra-stereo reconstruction, a SIFT/SURF feature based matching is used to obtain a list of sparse TPs followed by the afore-mentioned mutual shape refinement. TPs are used to rectify the left and right images into epipolar geometry. In the densification/stereo-matching step, a region growing/ALSC (Gotcha) based approach is used to produce dense disparity maps (Shin and Muller, 2012).

In the second stage, we build a wide baseline image network through 5 steps: (1) 3D triangulation from each intra-stereo pair. (2) Back project point clouds to each left image. (3) Define inter-stereo pairs. (4) Link TPs between inter-stereo pairs. (5) Link TPs between intra-stereo pairs. The image network defines inter-stereo pairs incrementally and is used as an initial link for all camera positions and orientations of a wide baseline area. The initial image network built in this stage will be adjusted progressively after inter-stereo matching and reconstruction.

In the third stage, inter-stereo reconstruction, we start by matching the inter-stereo images, i.e. left images of two intra-stereo pair and right images of two intra-stereo pair. The inter-stereo TPs are then densified by Gotcha matcher. In the next step, we transform the TPs from inter-stereo pairs back to the first intra-stereo image space incrementally. After triangulation of each intra-stereo pair from the first stage, the point clouds for each intra-stereo pair are linked via dense TPs from the inter-stereo matches. An initial wide baseline 3D point clouds are generated at this stage.

In the final stage, BA is used to correct the inter-stereo image network and update the extrinsic calibration data. The wide baseline 3D point clouds are then updated according to the adjustment between each inter-stereo pair progressively. For close range (<5 m), we are able to produce better than 10 mm/pixel resolution ORI/DTMs.

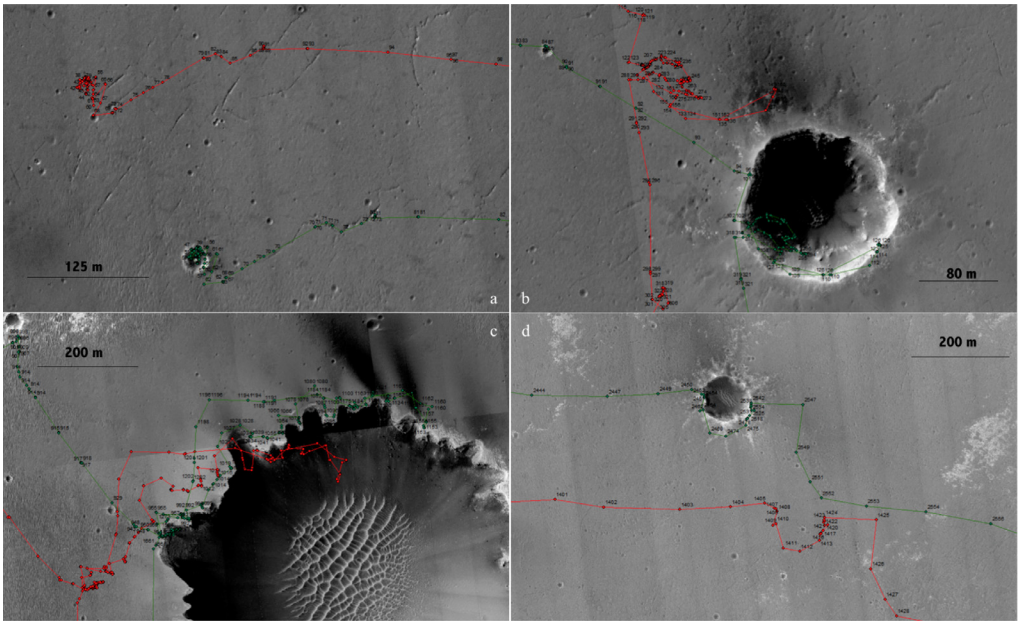

Fig. 22. Zoom-in view of corrected MER-B rover traverse (green) and initial IBA traverse (red) on HiRISE map (co-registered with CTX, HRSC, MOLA) at (a) Eagle crater, (b) Endurance crater, (c) Victoria crater, and (d) Santa Maria crater. North is up. (For interpretation of the references to colour in this figure legend, the reader is referred to the web version of this article).

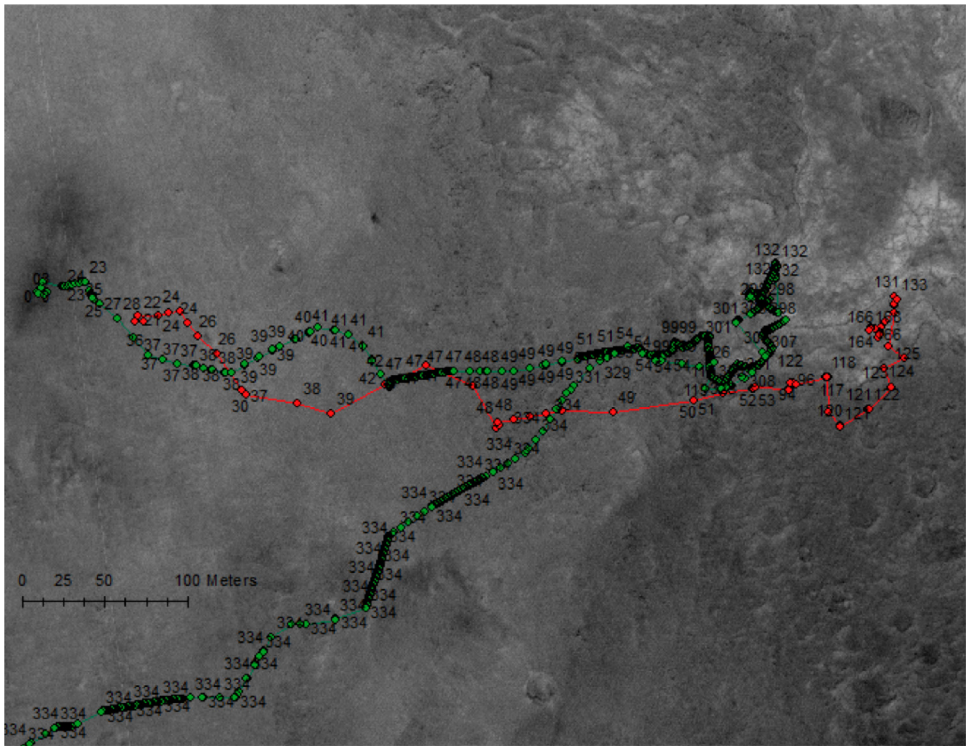

Fig. 23. Corrected MSL rover traverse (green) and initial telemetry traverse (red) on HiRISE map (co-registered with CTX, HRSC, MOLA). North is up. (For interpretation of the references to colour in this figure legend, the reader is referred to the web version of this article).

Landmarks such as craters, cliffs, and hills are the most important features to reconstruct for ground-to-orbit fusion. Wide baseline reconstructions of such areas can be more effectively co-registered with orbital ORI/DTMs. For MER-B, the data collected around, e.g. Eagle Crater (Sol 1–65), Endurance Crater (Sol 95–318), Victoria Crater (Sol 950–1683), and Santa Maria Crater (Sol 2450–2542), contains huge amounts of wide baseline panoramas with significant structural features that are viewable from HiRISE ORI/DTM. For MER-A, a similar situation appears around the Columbia Hills (Sol 155–581) and HomePlate (Sol 745–2180). For MSL, there are many wide baseline panoramas with rich feature appearing in Shaler (Sol 120 and 121), Yellowknife Bay

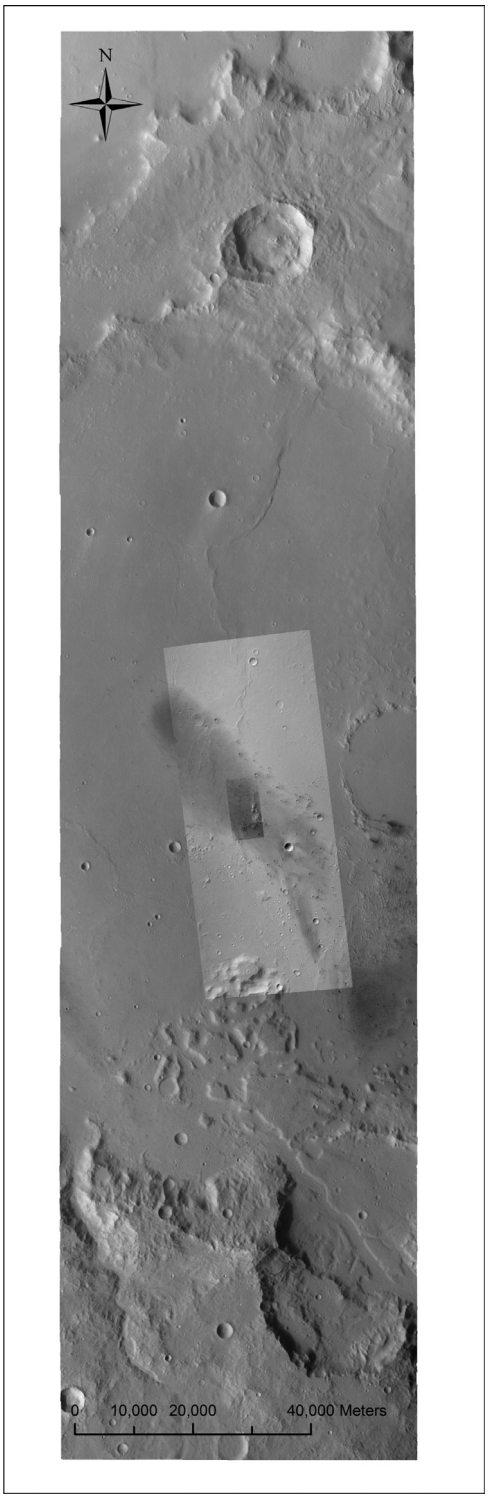

Fig. 24. The cascaded datasets created in this work for MER-A showing co-registered HiRISE ORI on top of the CTX and HRSC ORI ($H4165_0000_ND4$) which is co-registered with MOLA.

(Sol 124–299), Gillespie Lake (Sol 130–133) and Cumberland (Sol 274–295). Comparably smooth areas that do not contain aforementioned structural features, for example, the wide baseline ORI example of Sol 50–54 shown in Fig. 10, cannot be used for automated Navcam to HiRISE co-registration, because most of the ground features, such as rocks with diameter less than 150 cm, are not visible from HiRISE image. On the other hand, Fig. 11 shows an

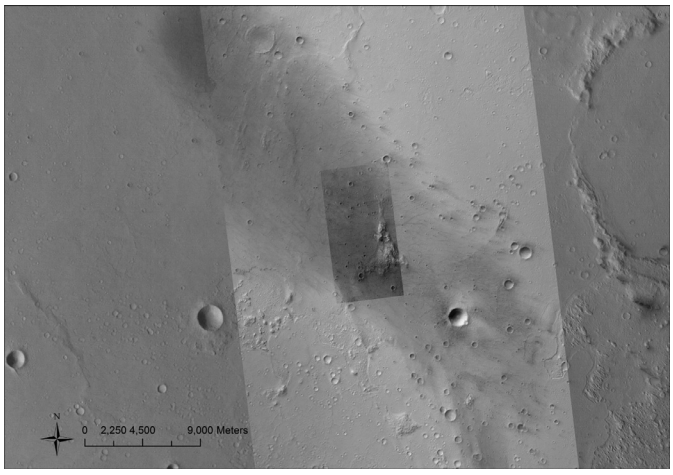

Fig. 25. A zoom-in view of the cascaded datasets for MER-A showing co-registered HiRISE ORI on top of the CTX and HRSC ORI ($H4165_0000_ND4$) which is co-registered with MOLA.

example of wide baseline Navcam ORI for Sol 127–131 that contains strong structural feature which are then used for Navcam to HiRISE co-registration shown in Fig. 16.

We initially search for serendipitous stereo pairs from the fulcra file derived from the raw Navigation and Ancillary Information Facility (NAIF) SPICE kernels. In this stage, computation of the approximated fulcra assumes a simple surface surrounding the rover. A SIFT/SURF based feature detection and matching process is employed where necessary for defining potential wide baseline panoramas. The fulcra file is subsequently updated applying the derived local DTMs or HiRISE DTMs after the BA and ground-to-orbit co-registration for further refinement of these field of view footprints. An example is given here in Fig. 12 showing intersections of image fulcra at Victoria Crater for cross-site reconstruction taken form the PRoGIS system.

4. Ground to orbit fusion

4.1. Co-registration of wide baseline ground ORI with HiRISE ORI

To relate close range views with global context views is critical in our localisation methods. We investigated several possible solutions including: (1) Fusing data in the 2D domain (multi-resolution/view image matching). (2) Fusing data in the 3D domain (3D data co-registration). (3) Fusing 3D data through 2D images (multi-dimensional and multi-resolution matching). Based on our experiments, fusion in the 2D domain is not feasible, since the scale and affine invariant image matching methods cannot be employed to solve the problem with significantly different wide baselines and resolutions. Fusion in 3D is conceptually straightforward as everything is done in the same dimension, see Fig. 13 and there are many existing point clouds registration algorithms, rigid and non-rigid, i.e. Iterative Closest Point (ICP), BA, or 3D scale invariant feature descriptors. However, going this way becomes computationally expensive and relies on robust point clouds denoising/filtering process. On the other hand, unless the rover goes into or close enough to a crater, any interesting structural features, i.e. crater edge or hill edge, normally appear in the mid or far range part of the Navcam DTM where the reconstruction quality and resolution is much lower. In the close range part, the local terrain is normally smooth and both spatial and vertical resolutions of the Navcam DTM are finer than the HiRISE DTM. Therefore it is very difficult to find any distinguishable correlations between them.

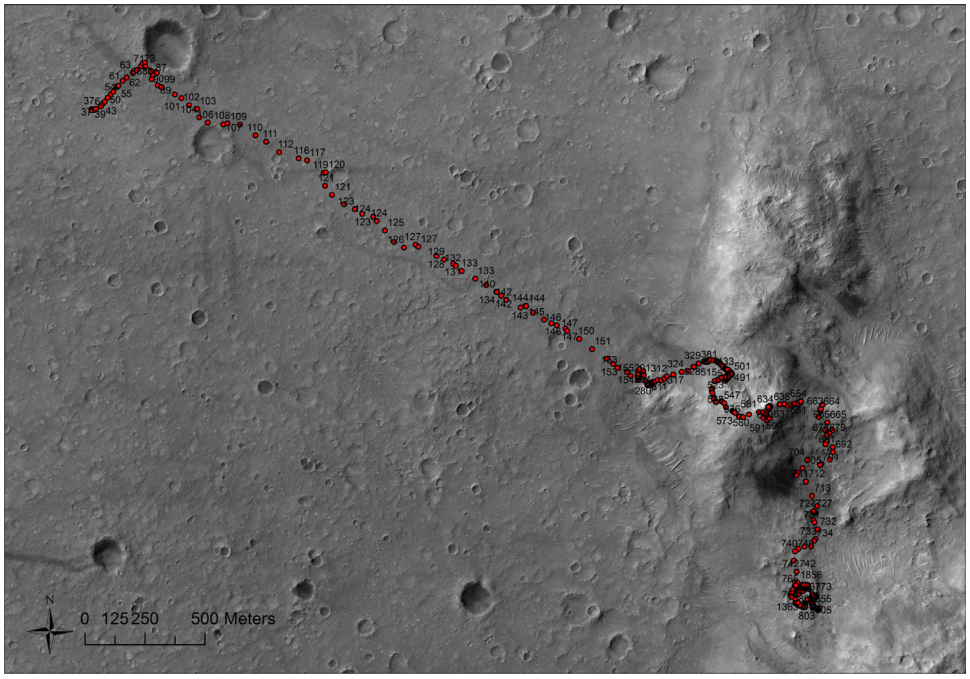

Fig. 26. A further zoom-in view of the cascaded datasets for MER-A showing the updated rover stops (red) and Sol numbers on top of the co-registered HiRISE ORI. (For interpretation of the references to colour in this figure legend, the reader is referred to the web version of this article).

Regarding the third option, there are two possible ways of fusing 3D via 2D images, i.e. re-project context ORI/DTM (HiRISE) onto the rover image plane, from which to establish 2D and 3D data connections, or orthorectify the ground rover image plane to be able to match with the orthorectified HiRISE image. The later approach is likely to be more feasible since in HiRISE, we have more information from the orthoview compared with re-projecting it to the rover image plane. In this work, a combined feature and area based registration method has been employed to achieve alignment of wide baseline Navcam ORIs and HiRISE ORI. The quality of the matching result depends on two key factors: (1) the wide baseline reconstruction covers a large enough area. (2) The area must have rich structural features. HiRISE ORI of smooth regions generally do not help to provide any matchable/viewable features for the Navcam ORI. For example, for MER-A, the region between Bonneville crater and Columbia hills is fairly smooth, a HiRISE ORI of this region may not help to provide any matchable feature with respect to wide baseline Navcam ORI.

We have described the wide baseline stereo reconstruction methods in the previous section. During the wide baseline reconstruction, in order to avoid inaccurate depth estimation from serendipitous Navcam stereo pair, the depth range was limited from –20 to 40 m. Also, the best reconstruction distance for producing less-distorted wide baseline Navcam ORI would be less than 15 m. In practice, we limited the cut-off distance from 10 to 25 m to pick up any extractable feature that could be matched with HiRISE ORI at 25 cm. Features further than 25 m are not useful as the spatial quality and resolution drops significantly.

The ground-to-orbit fusion processing chain is shown in Fig. 14. We initially use the information from raw traverse data in the rover reference system and landing site geographic coordinates in the global reference system to define a search area in HiRISE. The searching area does not necessarily need to be accurate but to maximize the automation of our processing chain. Alternatively, one can define the approximate area containing the reconstructed wide baseline ORI manually. The pre-processing includes a series of bilateral and Gaussian filtering kernels and interpolation processes, in order to initially smooth out noise generated in the Navcam reconstruction/orthorectification and local textures that do not appear in HiRISE. In the meantime, the structural texture that is likely to be apparent in HiRISE are preserved and initially enhanced in pre-processing. After pre-processing, the wide baseline Navcam ORI and HiRISE ORI (subset) are scaled into the same spatial resolution, i.e. 5 cm/pixel or 10 cm/pixel in general. The next step applies a morphological gradient transformation to further enhance the linear edge features in both of wide baseline Navcam ORI and HiRISE ORI.

The enhanced Navcam ORI and HiRISE ORI are then registered using normalised Mutual Information approach. Mutual information is determined from the joint histogram, which is computed over the overlapping area, with Navcam ORI mosaic moving through the HiRISE ORI clip with defined pixel precision and angular step size. We use the normalised form of mutual information in order to eliminate the effects of unreliable joint histograms caused by local texture. In other words, as the Navcam ORI mosaic moves away from the optimal registration window that is yielded by enhanced structural texture, mutual information could still increase if the increase of marginal entropies exceeds the decrease of the joint entropy between them. Radiometric differences are handled by a gradient descent approach to the least squares formulation. A first stage rigid transformation will be determined in this step. There is an optional cross checking step to look for local cross correlation of the derived gradient intensity. At this stage, the single rover position ORI that contains only panning motion of the cameras is located in the HiRISE ORI based on the aligned wide baseline ORI that contains this single position ORI. Perspective-SIFT features (Cai et al., 2013) are detected with the two aligned ORIs followed by a local ALSC refinement. The final transformation of the requisite position is determined based on the LSF of the local refinement result. The traverse covering the reconstructed wide baseline area is corrected after all positions have been refined.

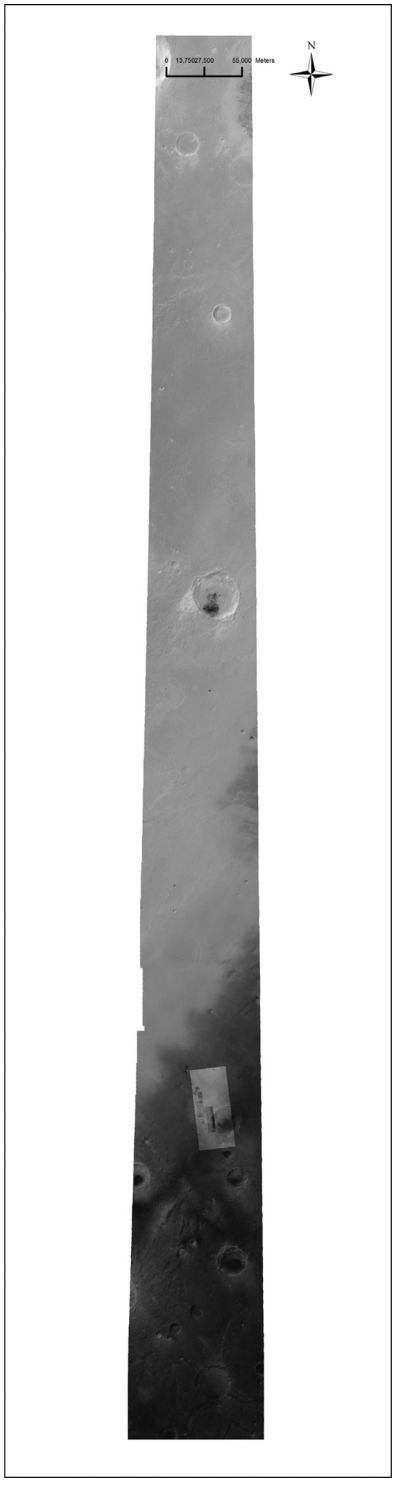

Fig. 27. The cascaded datasets created in this work for MER-B showing co-registered HiRISE ORI on top of the CTX and HRSC ORI ($H1183_0000_ND4$) which is co-registered with MOLA.

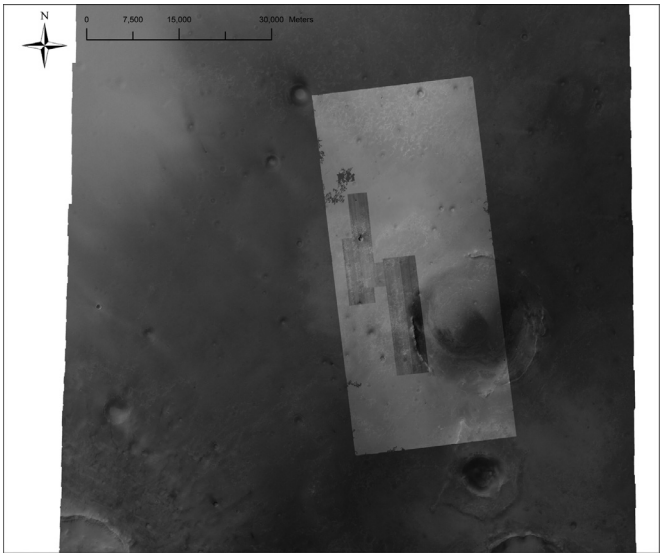

Fig. 28. A zoom-in view of the cascaded datasets for MER-B showing co-registered HiRISE ORI on top of the CTX and HRSC ORI ($H1183_0000_ND4$) which is co-registered with MOLA.

Considering the impact of smooth areas in the HiRISE image that we are not able to fuse with ground ORIs, only specific areas are searched for Navcam to HiRISE co-registration. The rover positions are then locked down for the areas where Navcam to HiRISE co-registrations can be performed. Rover positions between any two co-registered areas are directly transformed from the IBA or BA correction results. In this way, the rover positions within selected areas are accurately localised with respect to HiRISE-CTX-HRSC ORI. The accuracy of the rover positions between two co-registered areas are no longer a percentage of the distance from the landing site, but a percentage of half the distance between two co-registered areas. In this way, we take the advantages of IBA but reduce its accumulated error while the rover moves further away. In the future, more sites will be co-registered to replace the IBA/BA connection between two registered sites to improve the localisation accuracy.

Fig. 15a shows an example of the MER-B HiRISE ORI for site 80 to 82 at Victoria crater. The structural feature and local texture terms are illustrated in Fig. 15b. The co-registered wide baseline Navcam ORI mosaics for the same area are superimposed on the HiRISE ORI in Fig. 15c and d).

In this work, we received IBA corrected traverses for MER-A and MER-B from OSU. The IBA corrected traverses were used as initial input in our localisation process. For MER-B, the Navcam to HiRISE co-registration were performed for 11 sites at Endurance Crater, 5 sites at Victoria Crater, and 2 sites at Santa Maria Crater. For MER-A, the Navcam to HiRISE co-registration were performed for 2 sites whilst approaching Bonneville Crater and 5 sites at HomePlate. The IBA corrected traverses between co-registered areas were transformed directly.

For MSL, we use the traverse derived from SPICE kernels as initial input. It is taken from the raw telemetry data. However, the HiRISE ORI is rich in structural texture at site 5 Shaler, Yellowknife Bay, Gillespie Lake, and site 6 Cumberland up to the third PDS release in August 2013. The traverse is then corrected using BA based on the co-registered positions at Site 5 and 6. Fig. 16 shows an example of the co-registered MSL wide baseline Navcam ORI and HiRISE ORI from Sol 120 to 179.

HiRISE images captured at different times covering the same area for the three rover missions are collected, projected, and co-registered with CTX and HRSC at MSSL. Some of them contain rover tracks in different areas. The corrected traverses are validated by comparison of rover tracks appeared in different HiRISE images and the reconstructed rover traverse. An example of the comparison between corrected rover traverses and rover tracks appeared in HiRISE images is given in Fig. 19. For MER-A, there are not enough places containing matchable structural feature that appear in both HiRISE and Navcam ORI mosaic for us to do the co-registration. In such situations, we use an alternative workflow, shown in Fig. 17,

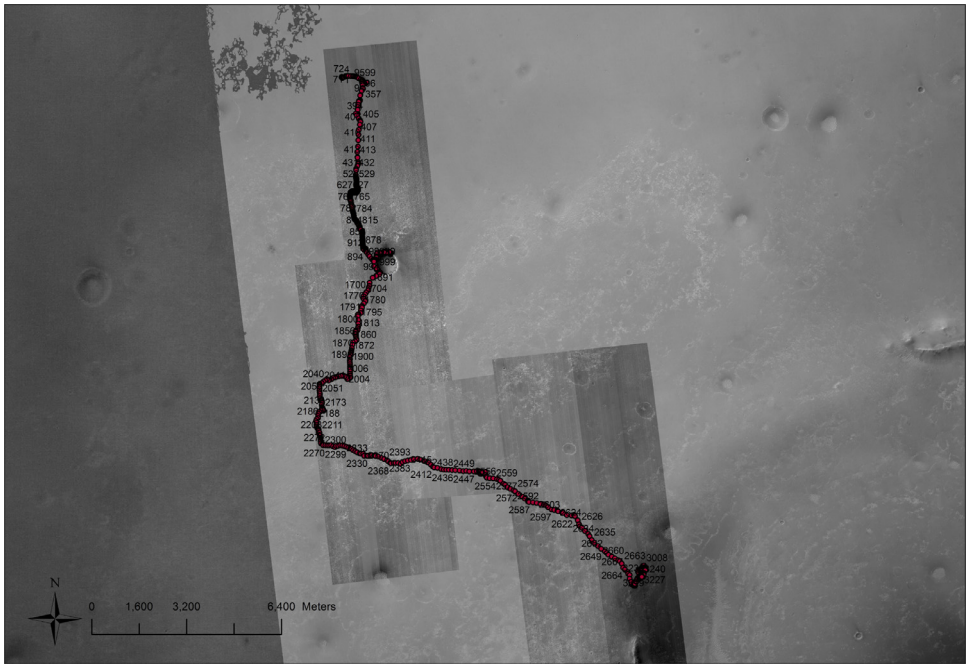

Fig. 29. A further zoom-in view of the cascaded datasets for MER-B showing the updated rover stops (red) and Sol numbers on top of the co-registered HiRISE ORI. (For interpretation of the references to colour in this figure legend, the reader is referred to the web version of this article).

to derive the rover track segments in different HiRISE images. Using the line-fitting method to match directly the rover tracks with rover traverse segments after IBA correction. An example of the fitted rover traverse at MER-A HomePlate is shown in Fig. 18. The traverse is cross-validated via different rover track segments appearing in different HiRISE images.

4.2. Updating rover traverse

The landing site coordinates after our localisation processing are 14.571166 degS 175.478431 degE for MER-A, 1.94726865 degS 5.52413974 degW for MER-B, and 4.589466952 degS 137.441633499 degE for MSL. The localisation results are presented in the Figs. 20–23, for MER-A (up to Sol 2169), MER-B (up to Sol 3240), and MSL (up to Sol 359), respectively.

5. Results

The localisation method introduced in this paper is based on experiments performed on data from the three U.S. rover missions and can be extended to future rover missions, e.g. the ESA 2020 ExoMars. We aim to produce accurate rover traverses with respect to a MOLA/HRSC reference framework using HiRISE-CTX-HRSC co-registration and an optimally combined method for Navcam-HiRISE co-registration using ground-to-orbit fusion and BA/IBA. The HiRISE and CTX ORI/DTMs are projected into Sinusoidal projection system to be consistent with the HRSC basemap. They are then co-registered with respect to the HRSC ORI using the automated HiRISE-CTX-HRSC co-registration method described in Section 2.3 in order to address the inconsistency issue described in Section 2.2. The rover traverses are then updated using the automated localisation method described in Sections 3.2 and 4.1.

The final results in this work are shown here and consist of the co-registered cascaded datasets that contain HRSC ORI/DTM, CTX ORI/DTM, HiRISE ORI/DTM, and updated rover positions for the three rover missions. Figs. 24–32 demonstrate the co-registered ORIs from HRSC, CTX, HiRISE and rover traverses for MER-A, MER-B and MSL, using the localisation and co-registration method described in this paper. All cascaded datasets are currently available to the PRoViDE project and published through an interactive web-GIS system which will be introduced in the next chapter.

6. Applications

6.1. Visualisation of multi-resolution 3D products from orbit to ground level

In order to make the results usable for geo-scientists, the co-registered orbital datasets and Navcam 3D products can also be directly and interactively explored and analysed using a 3D viewer developed by VRVis, a collaborator on the PRoViDE project (Tao et al., 2014; Traxler et al., 2014). The server-side 3D viewer, called PRo3D®, applies advanced real-time rendering methods to enable smooth navigation through 3D reconstructions of planetary terrains. The rover's elevation has been derived from the co-registered HiRISE DTM for the 3D visualisation in PRo3D®.

A very high degree of realism is important to allow geological assessments. To achieve this goal, physical properties of rock material are considered for rendering. Different Bidirectional Reflectance Distribution Functions (BRDFs) are estimated from source images and implemented as shaders that directly run on a Graphical Processing Unit (GPU) and hence in real-time at UCL-MSSL.

6.2. Interactive Web-GIS system for science target selection

In addition, an interactive web-GIS system, called PRoGIS[5], has been developed at the University of Nottingham in collaboration with UCL-MSSL (Morley et al., 2014). The co-registered HRSC-CTX-HiRISE and rover traverse datasets have been fully integrated into this web-GIS system, which will enable a virtual geologist to perform close-up visual analysis of key features (e.g. sedimentary layers) located in the global context and make measurements (e.g.

[5] http://www.progisweb.eu.

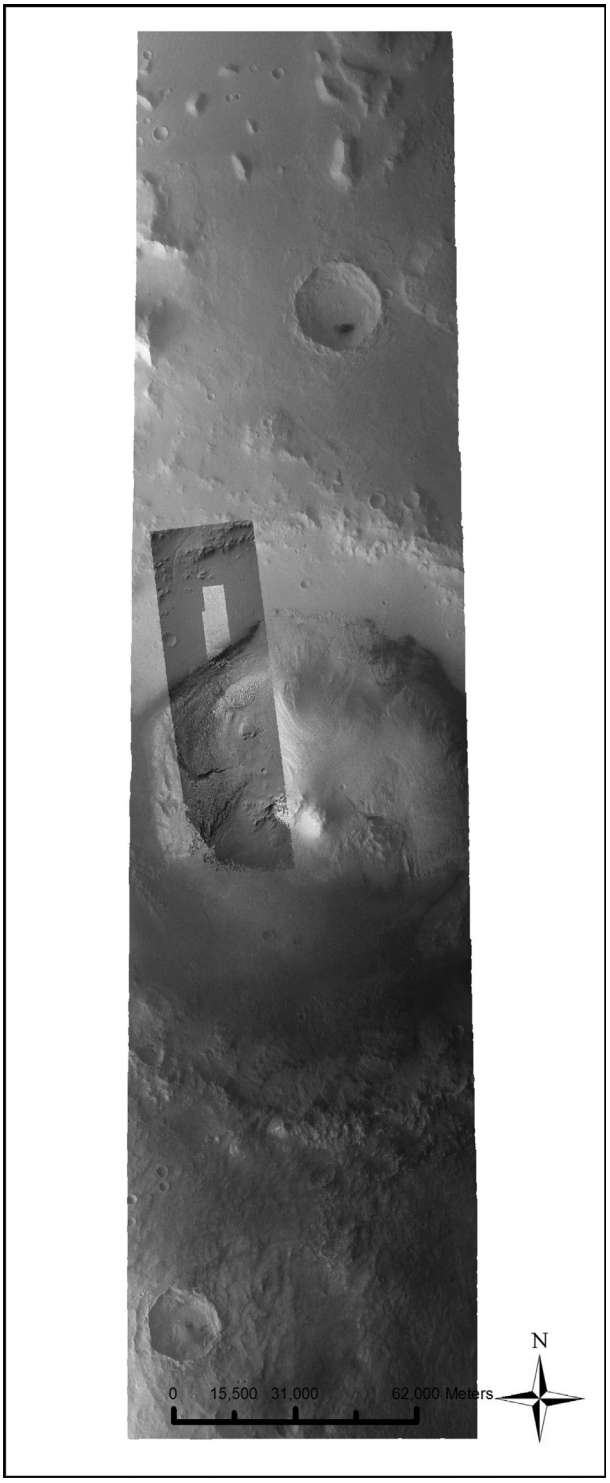

Fig. 30. The cascaded datasets created in this work for MSL showing co-registered HiRISE ORI on top of the CTX and HRSC ORI ($H1927_0000_ND4$) which is co-registered with MOLA.

distance, dip and slope) with different levels of detail. Scientists are able to select different geological features in global context and jump into a detailed local view of a 3D scene in PRo3D®. Access requests to PRoGIS can be made through the authors.

The planetary science community thus has access to processed products in this work and the original imagery from the Mars rover mission data (via UCL-MSSL PDS mirror) through PRoGIS. Additionally, PRoGIS also provides interactive photogrammetric operations,

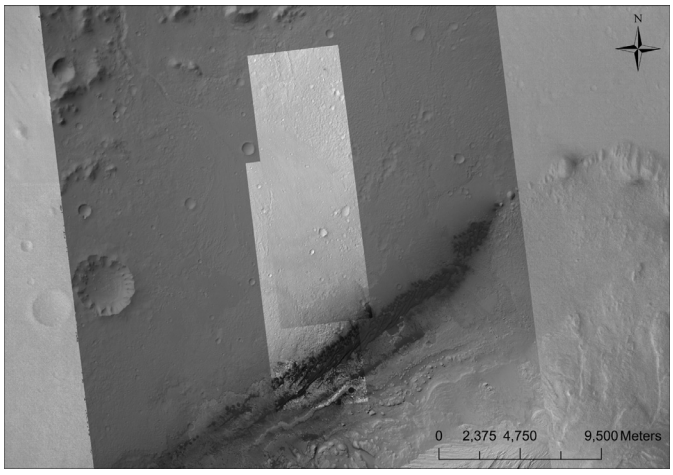

Fig. 31. A zoom-in view of the cascaded datasets for MSL showing co-registered HiRISE ORI on top of the CTX and HRSC ORI ($H1927_0000_ND4$) which is co-registered with MOLA.

which are powered by the PRoViP (Planetary Robotics Vision Processing) system developed by Paar and co-workers within PRoVisG, to initiate better understanding of the surface for expert users. PRoGIS will serve the educational, public outreach and scientific objectives of this work.

7. Conclusions and future work

In this paper, we introduced several new techniques and applications of automated optical co-registration based rover localisation methods showing examples from MER-A, MER-B, and MSL. New techniques include automated orbital dataset co-registration, wide baseline ground mapping, and ground to orbital co-registration. Our analysis has shown the mis-registration between publicly available HiRISE ORI/DTMs from the NASA HiRISE site and HRSC/MOLA with respect to the three rover missions, and introduced the consequences that the rover traverse (and the associated SPICE kernel data for each and every rover image acquired in local coordinates) does not match the landmarks observed in the HiRISE image after co-registration of HiRISE-CTX-HRSC. We developed an automated processing chain for retrieving rover locations through co-registration from orbital to ground co-ordinates to bring everything into the same unique and common georeferenced coordinate system with respect to HRSC, whose provenance is well documented with co-registration to MOLA (Scholten et al., 2005). Our method takes the advantage of improved localisation accuracy from IBA/BA, but avoids the inaccuracies associated with using the initial rover position obtained through triangulation of observations on orbital images and landing site surface images or UHF two-way Doppler tracking technology. In addition, our multi-sensor co-registration based method guarantees a global compliance that does not have accumulated error in network based localisation approaches. The results are a set of co-registered ORI/DTMs from HiRISE, CTX, and HRSC and updated rover locations for the full traverses of the three rover missions. They can be interactively explored and analysed using our 3D viewer and web-GIS system. The developed processing chains will be further employed in future rover missions, e.g. ESA ExoMars 2020. In the future, further SPICE kernel updates will be derived to be consistent with all datasets from orbit to ground level including the 3D surface of the planet.

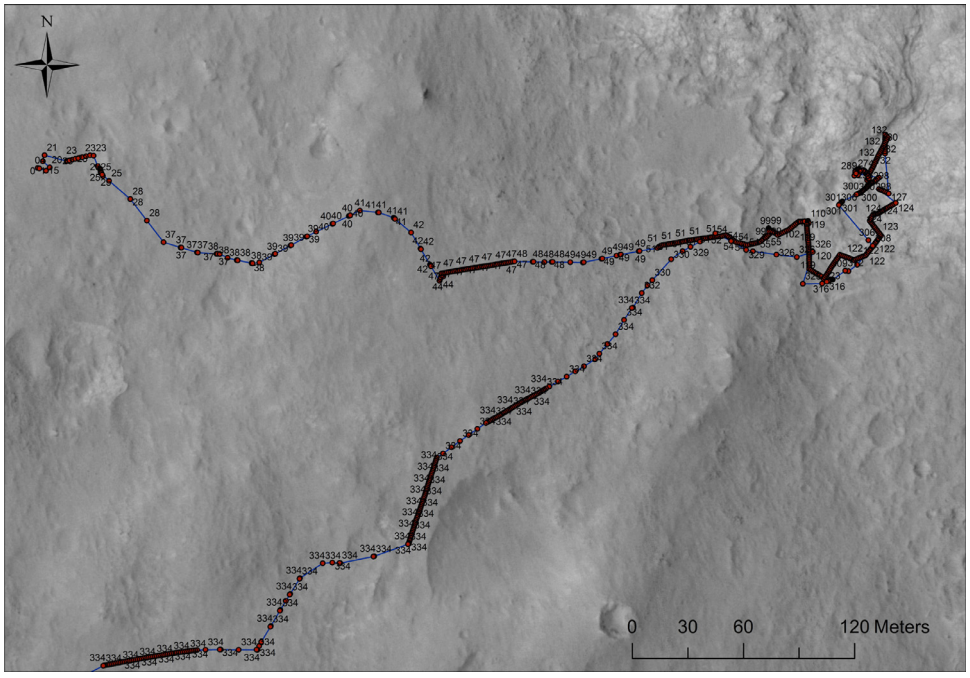

Fig. 32. A further zoom-in view of the cascaded datasets for MSL showing the updated rover stops (red) and Sol numbers on top of the co-registered HiRISE ORI. (For interpretation of the references to colour in this figure legend, the reader is referred to the web version of this article).

Acknowledgments

The research leading to these results has received funding from the European Community's Seventh Framework Programme (FP7/2007-2013) under grant agreement No.312377 PRoViDE as well as partial support for the second author under the STFC Consolidated grant, ST/K000977/1 and for W. Poole under the STFC PhD studentship, (ST/I506053/I).

References

Broxton, M.J., Edwards, L.J., 2008. The ames stereo pipeline: Automated 3-d surface reconstruction from orbital imagery. In: Proc. Lunar Planet. Sci. Conf XXXIX Abstract LPSC-2419.

Cai, G., Jodoin, P.-M., Li, S., 2013. Perspective-sift: An efficient tool for low-altitude remote sensing image registration. Signal Process. 93 (11), 3088–3110.

Guinn, J.R., 2001. Mars surface asset positioning using in-situ radio tracking. In: Proceedings of AAS/AIAA Space Flight Mechanics Meeting, pp. 45–54.

Guinn, J.R., Ely, T.A., 2004. Preliminary results of Mars exploration rover in situ radio navigation. In: Proceedings of AAS/AIAA Space Flight Mechanics Meeting, pp. 04–270.

Kim, J.-R., Muller, J.-P., 2009. Multi-resolution topographic data extraction from martian stereo imagery. Planet. Space Sci. 57, 2095–2112.

Kirk, R.L., Howington-Kraus, E., Rosiek, M.R., 2008. Ultrahigh resolution topographic mapping of Mars with MRO HiRISE stereo images: Meter-scale slopes of candidate phoenix landing sites. JGR 113.

Li, R., Archinal, B.A., Arvidson, R.E., et al., 2006. Spirit rover localization and topographic mapping at the landing site of Gusev Crater, Mars. JGR 111.

Li, R., Di, K., Wang, J., 2005. Incremental bundle adjustment techniques using networked overhead and ground imagery for long-range autonomous Mars rover localization. In: Proceedings of the 8th International Symposium on Artificial Intelligence, Robotics and Automation in Space (ISAIRAS).

Li, R., He, S., Chen, Y., et al., 2010. MER spirit rover localization: Comparison of ground image and orbital image based methods and science applications. JGR 116.

Li, R., Hwangbo, J., Chen, Y., 2011. Rigorous photogrammetric processing of HiRISE stereo imagery for Mars topographic mapping. IEEE Trans. Geosci. Remote Sens. 49 (7).

Li, R., Di, K., Matthies, L., 2004. Rover localization and landing-site mapping technology for the 2003 Mars exploration rover mission. Photogramm. Eng. Remote Sens. 70 (1), 77–90.

Maki, J., Thiessen, D., Pourangi, A., 2012. The Mars science laboratory engineering cameras. Space Sci. Rev 170, 77–93.

Malin, M., Caplinger, M., Edgett, K., et al., 2010. The Mars Science Laboratory (MSL) Mast-Mounted Cameras (Mastcams) flight instruments. In: Proc. 41st Lunar Planet. Sci. Conf Abstract LPSC-1123.

Matthies, L., Gat, E., Harrison, R., 1995. Mars microrover navigation: Performance evaluation and ehancement. Auton. Robots 2 (4), 291–311.

Morley, J., Sprinks, J., Muller, J.-P., 2014. Contextualising and analysing planetary rover image products through the web-based PRoGIS. In: Proceedings of Geophysical Research Abstracts (EGU), vol. 16.

Otto, G., Chau, T., 1989. Region-growing algorithm for matching of terrain images. Image Vis. Comput. 7 (2), 83–94.

Paar, G., Muller, J.-P., Tao, Y., 2013. Provide: Planetary probes mass vision data processing. In: Proceedings of European Planetary Science Congress (EPSC).

Parker, T.J., Malin, M.C., Calef, F.J., et al., 2013. Localization and contextualization of curiosity in gale crater, and other landed Mars missions. In: Proc. 44th Lunar Planet. Sci. Conf Abstract LPSC-2534.

Parker, T.J., Malin, M., Golombek, M., et al., 2004. Localization, localization, localization, reports. In: Proc. 35th Lunar Planet. Sci. Conf XXXV Abstract LPSC-2189.

Poole, W., Muller, J.-P., 2013. Mars us rover traverse co-registration using multi-resolution orbital 3d imaging datasets. In: Proc. Eur. Planet. Sci. Congr. (EPSC).

Scholten, F., Gwinner, K., Roatsch, T., et al., 2005. Mars express HRSC data processing: Methods and operational aspects: Mapping Mars. Photogramm. Eng. Remote Sens. 71, 1143–1152.

Shin, D., Muller, J.-P., 2012. Progressively weighted affine adaptive correlation matching for quasi-dense 3d reconstruction. Pattern Recognit. 45 (10), 3795–3809.

Tao, Y., Muller, J.-P., 2013. A multi-resolution 3d reconstruction tool: Exemplar using MSL navcam PDS and MastCam PIO imagery. In: Proceedings of European Planetary Science Congress (EPSC).

Tao, Y., Muller, J.-P., Willner, K., 2014. 3d data products and web-gis for Mars rover missions for seamless visualisation from orbit to ground-level. In: Proceedings of ISPRS Commission IV Symposium, vol. 8.

Traxler, C., Hesina, G., Gupta, S., 2014. An interactive virtual 3d tool for scientific exploration of planetary surfaces. In: Proceedings of Geophysical Research Abstracts (EGU), Vol. 16.

Xu, F., 2004. Automation in Mars landing-site mapping and rover localization. In: Proceedings of ISPRS Commission VI Symposium.

Xu, F., Ma, F., Li, R., 2001. Automatic generation of a hierarchical DEM for Mars rover navigation. In: Proceedings of the 3rd Mobile Mapping Conference.